Monthly Notices
of the
ROYAL ASTRONOMICAL SOCIETY

MNRAS **464,** 3385–3407 (2017)
Advance Access publication 2016 October 13

doi:10.1093/mnras/stw2633

How to design a planetary system for different scattering outcomes: giant impact sweet spot, maximizing exocomets, scattered discs

M. C. Wyatt,[1]★ A. Bonsor,[1] A. P. Jackson,[2] S. Marino[1] and A. Shannon[1,3,4]

[1] *Institute of Astronomy, University of Cambridge, Madingley Road, Cambridge CB3 0HA, UK*
[2] *School of Earth and Space Exploration, Arizona State University, 781 E Terrace Mall, Tempe, AZ 85287-6004, USA*
[3] *Department of Astronomy & Astrophysics, The Pennsylvania State University, State College, PA 16801, USA*
[4] *Center for Exoplanets and Habitable Worlds, The Pennsylvania State University, State College, PA 16802, USA*

Accepted 2016 October 12. Received 2016 October 1; in original form 2016 July 5; Editorial Decision 2016 October 11

ABSTRACT

This paper considers the dynamics of the scattering of planetesimals or planetary embryos by a planet on a circumstellar orbit. We classify six regions in the planet's mass versus semimajor axis parameter space according to the dominant outcome for scattered objects: ejected, accreted, remaining, escaping, Oort Cloud, and depleted Oort Cloud. We use these outcomes to consider which planetary system architectures maximize the observability of specific signatures, given that signatures should be detected first around systems with optimal architectures (if such systems exist in nature). Giant impact debris is most readily detectable for 0.1–10 $M_\oplus$ planets at 1–5 au, depending on the detection method and spectral type. While A stars have putative giant impact debris at 4–6 au consistent with this sweet spot, that of FGK stars is typically $\ll$1 au contrary to expectations; an absence of 1–3 au giant impact debris could indicate a low frequency of terrestrial planets there. Three principles maximize the cometary influx from exo-Kuiper belts: a chain of closely separated planets interior to the belt, none of which is a Jupiter-like ejector; planet masses not increasing strongly with distance (for a net inward torque on comets); and ongoing replenishment of comets, possibly by embedded low-mass planets. A high Oort Cloud comet influx requires no ejectors and architectures that maximize the Oort Cloud population. Cold debris discs are usually considered classical Kuiper belt analogues. Here we consider the possibility of detecting scattered disc analogues, which could be betrayed by a broad radial profile and lack of small grains, as well as spherical 100–1000 au mini-Oort Clouds. Some implications for escaping planets around young stars, detached planets akin to Sedna, and the formation of super-Earths are also discussed.

Key words: circumstellar matter – stars: formation – planetary systems.

1 INTRODUCTION

While the dynamics of extrasolar planetary systems can appear complex, a consideration of how Keplerian orbits are perturbed using the disturbing function shows that it is usually possible to consider dynamical interactions as the sum of three distinct types of perturbation (see Murray & Dermott 1999): resonant perturbations that act when the ratios of orbital periods are close to a ratio of two integers, secular perturbations that act over long time-scales at all locations in the system, and short-period perturbations that usually average to zero but become important when objects undergo close encounters (i.e. scattering). For many populations of small bodies in planetary systems, and indeed the planetary system itself, the dynamical evolution is dominated by one type of perturbation. For example, since secular perturbations are unavoidable, these perturbations are often dominant (Wyatt et al. 1999; Lee & Peale 2003). However, for many populations, resonances are also important (Fabrycky & Murray-Clay 2010; Batygin 2015), even if the objects are not actually in resonance (e.g. Rasio et al. 1992).

Here we propose a framework within which to consider the outcomes of scattering processes. The pioneering work of Tremaine (1993, hereafter T93), itself based on previous work such as that of Duncan, Quinn & Tremaine (1987), showed how the ultimate fate of any test particles encountering and subsequently being scattered by a planet depends on the planet's mass and semimajor axis. Thus, T93 showed that the planet mass versus semimajor axis parameter space could be divided into regions with different outcomes. That work focused on the possibility of implanting comets in the Oort Cloud, and that has also been the emphasis of subsequent work

★ E-mail: wyatt@ast.cam.ac.uk

that extended this analysis. For example, Brasser & Duncan (2008) showed how additional constraints can be placed in this parameter space, which depends on the eccentricity of the planet's orbit (which is ignored here in the first instance), and gave consideration to multiple planet systems (which we will consider later).

However, the value of the division of parameter space in this way extends beyond the formation of Oort Clouds. Indeed, this parameter space outlines the likely outcome for a particle undergoing repeated encounters with that planet. Many dynamical populations evolve in a manner that is dominated by multiple scatterings with planets. This applies to any objects that are on planet-crossing orbits, although secular and resonant perturbations can also become important in this regime (e.g. Levison & Agnor 2003; Beust et al. 2014; Tamayo 2014). Generally speaking, the scattered population is made up of either objects that were either born on planet-crossing orbits or those for which perturbing forces nudged them on to planet-crossing orbits at a later date. In the Solar system, the most obvious scattered population is the comets (e.g. Duncan & Levison 1997). This includes both objects born in the vicinity of the planets that have been evolving ever since through scattering, including the placement in the Oort Cloud (e.g. the long-period comets), and those born on quasi-stable orbits far from planets, but which have more recently been perturbed on to planet-crossing orbits (e.g. the Jupiter-family comets). Other small-body populations are also expected to follow this type of evolution. For example, in the inner Solar system, debris that is born on planet-crossing orbits includes that created in the giant impact which created the Earth's Moon (Canup & Asphaug 2001), while debris that is perturbed on to planet-crossing orbits at a later date includes the near-Earth asteroids (Bottke et al. 2002).

Analogy with the Solar system means that scattering processes may also apply to small bodies such as asteroids and comets orbiting within extrasolar planetary systems. Such small bodies are known to be present around many nearby stars from the detection of circumstellar dust known as a debris disc that is created as these larger planetesimals are destroyed (e.g. Wyatt 2008). If scattering processes are at play in these systems, then the structure of their debris discs may bear the imprint of those scattering processes. Indeed, there are several systems for which it is proposed that debris has been seen following a giant impact on to a planet which controls the subsequent evolution of that debris (e.g. Lisse et al. 2012), and there is mounting evidence for the existence of exocomets (e.g. Beichman et al. 2005; Kiefer et al. 2014; Boyajian et al. 2016). Furthermore, while most known debris discs are usually considered to be classical Kuiper belt analogues, in that they comprise objects that orbit far enough from planets to not undergo strong encounters, the possibility of strong scattering is brought home by the discovery of the Fomalhaut system in which a planet-like object is seen to be on an orbit that crosses the debris belt (Kalas et al. 2013).

It is also thought that planets themselves undergo epochs of intense scattering. Such a rearrangement of the planets has been proposed in the Solar system to explain the moderate orbital eccentricities of the giant planets (e.g. Tsiganis et al. 2005). The high eccentricities of the giant planets of extrasolar planetary systems have likewise been proposed to originate in an epoch of planet–planet scattering (e.g. Chatterjee et al. 2008; Jurić & Tremaine 2008). Many aspects of the scattering evolution discussed in this paper will also apply to populations of larger bodies, and so the framework discussed herein can also be used to consider some aspects of the dynamical evolution of, say, scattered planetary embryos.

In Section 2, we replicate the division of parameter space as presented in T93, with only minor modifications, but give equal consideration to outcomes other than the formation of an Oort Cloud.

Table 1. Units of parameters introduced in Section 2.

Parameter	Symbol	Units
Stellar luminosity	$L_\star$	$L_\odot$
Stellar mass	$M_\star$	$M_\odot$
Planet mass	M_p	$M_\oplus$
Planet semimajor axis	a_p	au
Oort Cloud radius	a_f	au
Ejection semimajor axis	a_{ej}	au
Local mass density	ρ_0	0.1 $M_\odot$ pc^{-3}
Planet density	ρ_p	1 g cm^{-3}
Stellar age	$t_\star$	Gyr

Then in Section 3, we show what the parameter space looks like for four specific cases which are also used to corroborate the ability of the model to make predictions for the outcome of numerical simulations of scattering processes in the literature. In Section 4, we then use the parameter space division to consider how to design planetary system architectures to maximize specific outcomes. Whether such planetary system architectures exist in nature is another matter, but throughout this paper, we refer to observations of extrasolar planets, Solar system minor planets, and extrasolar debris discs to which this method may be applied. Conclusions are given in Section 5.

2 PLANET MASS VERSUS SEMIMAJOR AXIS PARAMETER SPACE

Consider a planet of mass M_p on a circular orbit around a star of mass $M_\star$ with a semimajor axis a_p. Throughout this paper, we assume that M_p is in $M_\oplus$, $M_\star$ is in $M_\odot$, and a_p is in au; the units used in this paper are summarized in Table 1. Fig. 1 shows the parameter space that is most important for determining the outcome of scattering interactions with that planet, i.e. planet mass versus semimajor axis. In Section 2.1, we describe the populations of known planets shown in Fig. 1, which includes both Solar system and extrasolar planets, as well as the debris populations (which are not shown). The shading in Fig. 1 shows six different regions of parameter space that are defined by the most likely outcome for planetesimals encountering a planet in that region of parameter space (assuming it is the only planet in the system): accreted (planetesimal ends up colliding with the planet), ejected (planetesimal ends up being ejected from the system), remaining (planetesimal remains in the system), escaping (planetesimal will soon be ejected but is currently still undergoing scattering), Oort Cloud (planetesimal ends up in the Oort Cloud), and depleted Oort Cloud (planetesimal was put in the Oort Cloud but has subsequently been ejected). This division is guided by lines that were derived in T93, and described in Sections 2.2, 2.3, and 2.4. More specifically, Fig. 1 shows how the parameter space is divided for the Solar system, i.e. for planets orbiting a 4.5-Gyr-old 1-$M_\odot$ star in a stellar environment with local mass density 0.1 $M_\odot$ pc^{-3}; thus, this figure is directly comparable with fig. 2 of T93, with mostly cosmetic changes. Note that this figure is not intended to show the only outcome for encounters with such planets. Rather the shading represents the expected dominant outcome, with the caveat that the dominant outcome may also be influenced by the initial parameters of the planetesimal's orbit as well as other planets in the system.

2.1 Planet and debris parameters

One of the cosmetic improvements to Fig. 1 that was not available to T93 is the addition of known exoplanets. Here we took the known

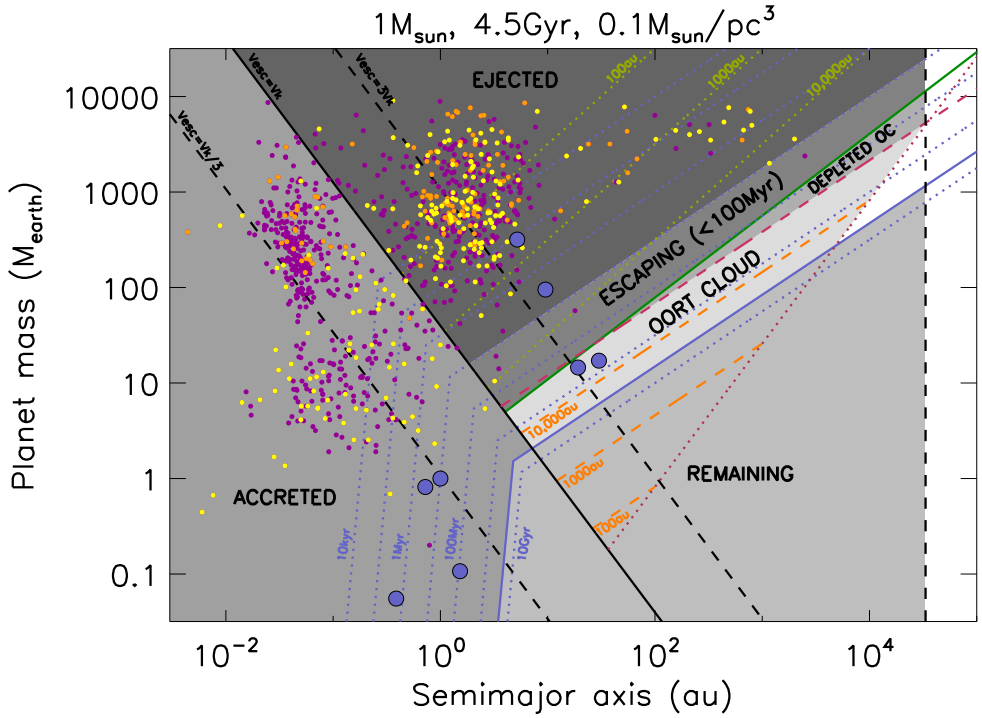

Figure 1. Planet mass versus semimajor axis parameter space. The yellow, purple, and orange dots show the known exoplanets found around $M_\star < 0.6$, $0.6 < M_\star < 1.4$, and $M_\star > 1.4$ stars, respectively; blue dots are the Solar system planets. The shading shows the dominant outcome of scattering interactions with a planet of given parameters (and density 1 g cm^{-3}) orbiting a 1-M$_\odot$ star for 4.5 Gyr of evolution in an environment with mass density 0.1 M$_\odot$ pc^{-3}. The time-scales to achieve these outcomes are given by the blue dotted lines (equations 2 and 3); the solid blue line corresponds to 4.5 Gyr. The semimajor axes at which planets eject particles are shown with yellow dashed lines (equation 4), and those at which particles are implanted in the Oort Cloud are shown with orange dashed lines (equation 5). The black diagonal lines correspond to planets with a constant ratio of escape velocity to Keplerian velocity (equation 1). The red dashed line is that at which stellar encounters strip particles from the Oort Cloud (equation 7), and the vertical black dashed line is the radius at which these encounters would have removed the planet over the system age (equation 10).

exoplanets from the NASA exoplanet archive (Akeson et al. 2013)[1] on 2016 February 25. The planets are coloured by the mass of their host star (yellow for $M_\star < 0.6\,\mathrm{M}_\odot$, purple for $0.6 < M_\star < 1.4\,\mathrm{M}_\odot$, and orange for $M_\star > 1.4\,\mathrm{M}_\odot$). The Solar system planets are also shown as the larger blue circles. This does not necessarily include all known exoplanets but serves to illustrate the main features of the exoplanet population.

The main populations are (see Udry & Santos 2007) as follows: (i) the hot Jupiters centred around $1M_{\rm jup}$, 0.03 au, which are found around ∼1 per cent of stars; (ii) the super-Earths centred around $10\,\mathrm{M}_\oplus$, 0.03–1 au, which are found around 30–50 per cent of stars; (iii) the eccentric Jupiters centred around a few $M_{\rm jup}$, 3 au, which are found around ∼5 per cent of stars; and (iv) the long-period giants that are $\sim 10M_{\rm jup}$ at >10 au, found around a few per cent of stars (Bowler 2016). Detection biases mean that true terrestrial planets and Neptune analogues are rare in the exoplanet population so the ubiquity of such planets is unknown at present. Estimates of these populations can be made, however, either by extrapolation of the super-Earth population (Howard et al. 2010) or from the small numbers of microlensing detections (Sumi et al. 2010).

Over the last 20 years, there has been a significant enhancement in our understanding of the populations of debris (i.e. the planetesimals which may be scattered by planets) around nearby stars, and indeed our own Sun (for reviews see Wyatt 2008; Matthews et al. 2014a). This paper will summarize the main populations. Approximately 20 per cent of Sun-like stars, and a similar, if not higher, fraction of A stars, host cold debris belts that are detected in the far-infrared (far-IR; Eiroa et al. 2013; Thureau et al. 2014, Sibthorpe et al., in preparation). These all have large inner holes that are empty of dust and when imaged are often shown to be radially confined to narrow rings, although broad discs covering a factor of a few in radius are also known. The inner holes have radii in the range of 10–150 au, with some obvious selection biases towards larger discs in those that can be imaged. Thus, these are considered to be exo-Kuiper belts. However, whether these are analogues to the classical Kuiper belt (i.e. objects born on stable orbits) or to the scattered disc (i.e. objects undergoing scattering with planets) is not much discussed. The longevity of some discs (e.g. HD 207129, Löhne et al. 2012), and the narrowness of others (e.g. Fomalhaut, Kalas, Graham & Clampin 2005), argues for a classical Kuiper belt interpretation for these systems, while broad discs seen around young stars could have a scattered disc interpretation. The azimuthal structure seen towards several imaged discs is a strong clue to the dynamics of these populations, and for some discs with a clumpy structure, this has been used to argue for a population analogous to the resonant Kuiper belt objects that were trapped in resonance with a migrating planet (Wyatt 2003; Dent et al. 2014).

Less frequently the inner regions of planetary systems are also seen to host abundant debris. In some cases, the hot dust is the only debris component present in the system at detectable levels (Beichman et al. 2005), but there are a number of debris discs with spectral energy distributions suggesting two temperatures of debris (Wyatt et al. 2005; Morales et al. 2009; Chen et al. 2014;

[1] http://exoplanetarchive.ipac.caltech.edu/

Kennedy & Wyatt 2014). The origin of this hot dust is a matter of considerable debate. Possibilities include the following: (i) These are analogues to the asteroid belt, although this is unlikely for old systems with dust $\ll$3 au, since such belts would have been depleted by collisional erosion (Wyatt et al. 2007a). (ii) This is dust released in a recent giant impact (Rhee, Song & Zuckerman 2008; Lisse et al. 2009; Jackson & Wyatt 2012), possibly similar to the Earth's Moon-forming collision. (iii) This is dust dragged in from the outer Kuiper belt by Poynting–Robertson drag (Mennesson et al. 2014; van Lieshout et al. 2014; Kennedy & Piette 2015). (iv) The dust is released from a comet-like population, either scattered in from an exo-Kuiper belt (Nesvorný et al. 2010; Bonsor, Augereau & Thébault 2012), or from a population analogous to the long-period comets (Beichman et al. 2005; Wyatt et al. 2010).

Our ability to know the dynamics of the planetesimal populations in specific systems is hampered by the fact that usually there is little information on the exoplanet system within which they reside. Nevertheless, a growing number of systems host planets and debris (Wyatt et al. 2012; Kalas et al. 2013; Kennedy & Wyatt 2014; Moro-Martín et al. 2015). Perhaps the most famous planet plus debris system is HR 8799 (Marois et al. 2008; Su et al. 2009), which will be considered in more detail in Section 3.3.

2.2 Maximum kick: accretion versus ejection

One of the most important lines in Fig. 1 is that for which the planet's escape velocity $v_{\rm esc}$ is equal to its Keplerian velocity $v_{\rm k}$ (e.g. Ford & Rasio 2008). Remembering the units given in Table 1, this can be found from the following relation between planet and stellar properties and the ratio $v_{\rm esc}/v_{\rm k}$:

$$M_{\rm p} = 40 M_\star^{3/2} a_{\rm p}^{-3/2} \rho_{\rm p}^{-1/2} (v_{\rm esc}/v_{\rm k})^3, \quad (1)$$

where the planet's density $\rho_{\rm p}$ is in units of 1 g cm^{-3}, and is assumed to be 1 g cm^{-3} for figures in this paper. The significance of this boundary is that the maximum velocity kick that a particle can receive in a single encounter with the planet is $v_{\rm esc}/\sqrt{2}$, since larger kicks require larger deflection angles that are possible only by approaching the planet with a smaller impact parameter, which would result in a collision. Assuming an initially circular orbit, a kick of the order of the Keplerian velocity is sufficient to put the particle on an unbound trajectory (if it is oriented in the right direction). Thus, equation (1) gives the approximate limit at which particles can be put on unbound trajectories in a single encounter. Since many more encounters are expected with deflection angles just below this limit than those above (i.e. with impact parameters at larger distances), one can expect that the further to the right of this line a planet is, the more kicks an object receives that can eject it from the system before it has an encounter that is close enough to collide with the planet; that is, collisions with the planet become unlikely as an outcome compared to the ejection of the object. Conversely, the further to the left of this line a planet is, the more likely an object is to collide with the planet before it receives sufficient kicks to increase its eccentricity so that its orbit evolves in a cometary diffusion regime.

This argument is phrased slightly differently from that presented in T93, which considered the collisional lifetime for objects in the cometary diffusion regime, but equation (14) of T93 has the same scaling and is identical to equation (1) within a factor of 2. Also shown in Fig. 1 for reference are the planets for which $v_{\rm esc}/v_{\rm k}$ is 1/3 and 3.

Thus, the conclusion is that, in the absence of other considerations, the eventual fate of objects to the left-hand side of the line is accretion on to the planet, while that of objects to the right-hand side of that line is ejection from the system. This is broadly in agreement with, for example, the simulations of Raymond, Armitage & Gorelick (2010), who showed that Jupiter-mass planets are more likely to lead to ejections, while lower mass planets are more likely to collide (see their fig. 4). The multiplanet N-body simulations of Veras et al. (2016) also exhibit a clear difference between the fates of scattered planets that started in different regions of Fig. 1; for example, 70/82 of their high-mass planets (Jupiters and Saturns that lie in the ejection regime) that leave the simulations are ejected (see their table A12), whereas of their Uranus- and Neptune-mass planets (that start in or close to the accretion regime) that leave the simulations, 8/33 are ejected and 9/33 collide with one another (see their table A13).

2.3 Timescale: remaining versus lost

The discussion in Section 2.2 for the eventual fate of scattered particles does not account for the time-scale for the ejection and accretion outcomes to occur. Thus, another important line in Fig. 1 is that for which the time-scale for these outcomes is the age of the system (which is the solid blue line).

For the region to the right-hand side of the line described by equation (1), that is, for particles for which the eventual outcome is ejection, the outcome time-scale is taken to be the cometary diffusion time, as empirically derived in T93 (their equation 3), and later derived analytically in Brasser & Duncan (2008) (see their appendix A). Thus, the planet parameters for which ejection occurs on a time-scale $t_\star$ in Gyr are given by

$$M_{\rm p} = M_\star^{3/4} a_{\rm p}^{3/4} t_\star^{-1/2}. \quad (2)$$

Fig. 1 shows with dashed blue lines the planets for which ejection occurs on different time-scales, as given in the annotation, and with the solid blue line that for which ejection occurs on a time-scale of the assumed age of the system $t_\star = 4.5$ Gyr.

For the region to the left-hand side of the line described by equation (1), that is, for particles for which the eventual outcome is accretion, the outcome time-scale is taken to be the collision time under the assumption that the relative velocities at which the particles encounter the planet are of the order of the escape velocity of the planet. More specifically, we consider an outcome time-scale that might be expected from debris released in a giant impact, and so use a relative velocity distribution scaled by the planet's escape velocity to that expected for ejecta released in the Moon-forming collision, further assuming an axisymmetric spatial distribution (see Jackson & Wyatt 2012). This results in a gravitational focusing factor which is the same for all planets (Wyatt & Jackson 2016), and means that the planet parameters for which accretion occurs on a time-scale $t_\star$ are (using equation 11 of Jackson & Wyatt 2012, with $\Delta v = v_{\rm esc}$) given by

$$M_{\rm p} = 10^{-6} M_\star^{-3} a_{\rm p}^{12} \rho_{\rm p}^{5/2} t_\star^{-3}, \quad (3)$$

and similar lines to those for the ejection outcome are plotted on Fig. 1. For example, equation (3) shows that debris from giant impacts involving the Earth, or those involving Mercury, is reaccreted on to those planets on time-scales of $\sim$10 and $\sim$0.6 Myr, respectively (for the nominal assumption of $\rho_{\rm p} = 1$ g cm^{-3}, and a factor of a few longer for their actual densities).

While the above assumptions mean that the time-scale given by equation (3) is most applicable to giant impact debris, a relative velocity that is comparable to the planet's escape velocity may also be a reasonable estimate for debris that is being stirred by the planet. However, stirring by other planets could set a higher relative

velocity for the debris, in which case the lines in Fig. 1 would have a shallower dependence on a_p.

Since the two lines described by equations (2) and (3) are not equal at the boundary given by equation (1), this would result in the appearance of a discontinuity at that line (which is avoided in Fig. 1 by showing the lines up to the point where they intersect). Clearly the approximations used to delineate the different outcomes, and to quantify the time-scales for those outcomes, break down close to the boundaries (e.g. equation 11 of Jackson & Wyatt 2012, who used an expansion applicable only for small $\Delta v/v_k$ and, furthermore, assumed a toroidal distribution of debris). This emphasizes the point that Fig. 1 should only be used as a guide to indicate the expected outcome and its time-scale, and that more detailed numerical simulations are needed, in particular to assess the outcomes near the boundaries. In any case, the assumption here is that objects below the solid blue lines have not had sufficient time to achieve their eventual fate described in Section 2.2, and so this region is labelled as remaining.

2.4 Tide: Oort Cloud versus ejected

T93 show how the eventual outcome in the region that would have been considered to result in ejection by the above reasoning can instead result in the particles being deposited in the Oort Cloud. This is because as the objects undergo cometary diffusion, that is, keeping their pericentres close to the planet but receiving kicks which increase their semimajor axes, they would be expected to be ejected after they reach a semimajor axis a_{ej} (in au) at which the individual kicks they receive when encountering the planet are sufficient to unbind them from the system. This means that planets of different masses eject particles after they reach different distances, as indicated with the yellow dotted lines in Fig. 1, given by (see equation 8 of T93)

$$M_p = 3 \times 10^4 M_\star a_p a_{ej}^{-1}. \quad (4)$$

However, the diffusion takes place on a finite time-scale that depends on the semimajor axis that the particle has reached, and there are additional perturbations to the particle's orbit from the Galactic tide and from stellar encounters, the time-scales for which also depend on the semimajor axis (see Heisler & Tremaine 1986). Since both tides and encounters can act to raise the particle's pericentre, this would stop the cometary diffusion and freeze the particle's semimajor axis at whatever value it has reached at that time, thus depositing it in the Oort Cloud (Duncan et al. 1987). In Appendix A, we show that, unless the object being scattered is orbiting a massive star (see equation A5), the relevant time-scales for Galactic tides are shorter than those of stellar encounters, and so the latter can be neglected in the following analysis. Thus, the semimajor axis at which this freezing occurs, a_f (in au), is the location at which the tidal time-scale equals that for cometary diffusion, and the orange dashed lines in Fig. 1 show the planets that result in freezing at different Oort Cloud sizes given by (rearranging equation 7 of T93)

$$M_p = 0.8 \times 10^{-3} M_\star^{1/2} a_p^{3/4} a_f^{3/4} \rho_0^{1/2}, \quad (5)$$

where ρ_0 is the local mass density in units of that near the Sun of 0.1 $M_\odot$ pc^{-3} (Holmberg & Flynn 2000).

Comparing the lines given by equations (4) and (5), it is clear that there is a line in Fig. 1 above which a particle is ejected before it can reach the semimajor axis at which it would be implanted in the Oort Cloud. This is shown in green in Fig. 1 and corresponds to (see equation 9 of T93)

$$M_p = 1.5 M_\star^{5/7} a_p^{6/7} \rho_0^{2/7}. \quad (6)$$

Ejection is the outcome above this line, and the yellow dotted lines show the semimajor axis at which ejection occurs (equation 4). While the outcome for particles encountering all planets above the green line should be *ejected*, we further subdivide this ejection outcome to include an *escaping* region to emphasize that the time-scale for ejection can be relatively long in this region, and so it is possible to see particles in the process of being ejected. The motivation for this area of parameter space will become clear in Section 3.3. Below the green line the eventual outcome would be for particles to be implanted in the Oort Cloud, which would be at a radius given by the orange dashed lines (equation 5), but noting that the time-scale to reach this outcome could be longer than the age of the system for low-mass planets.

Two other lines are shown in Fig. 1 relating to the Oort Cloud outcome. One is that for which the half-life for objects in the Oort Cloud due to perturbations from passing stars is equal to the age of the system, which is shown as the red dashed line, given by (see equation 16 of T93)

$$M_p = 7 M_\star^{3/4} a_p^{3/4} \rho_0^{-1/4} t_\star^{-3/4}. \quad (7)$$

Above this line, objects may be implanted in the Oort Cloud (if the planet is not massive enough to eject the particles before they reach this location), but they would be subsequently removed by the passage of nearby stars; that is, the ultimate fate of particles encountering planets in the depleted Oort Cloud region is ejection, though some fraction may remain in a depleted Oort Cloud.[2] The other line is the red dotted line, which is that for which the semimajor axis at which the planet would implant objects in the Oort Cloud is equal to that of the planet itself (see equation 13 of T93):

$$M_p = 0.8 \times 10^{-3} M_\star^{1/2} a_p^{3/2} \rho_0^{1/2}. \quad (8)$$

Clearly a planet to the right-hand side of this line could not form an Oort Cloud.

Finally, planets are not considered if they are either outside the tidal radius of the star (see equation 10 of T93), which is those beyond

$$a_p = 1.9 \times 10^5 M_\star^{1/3} \rho_0^{-1/3}, \quad (9)$$

or if they have a half-life due to perturbations from passing stars that is shorter than the system age (see equation 15 of T93), which is those beyond

$$a_p = 1.5 \times 10^5 M_\star \rho_0^{-1} t_\star^{-1}. \quad (10)$$

Equations (9) and 10 are shown with vertical black dotted and dashed lines, respectively, in the figures (when they fall within the plotted range).

2.5 Applicability to scattered planets

The division of parameter space described in this section applies specifically to the scattering of test particles, that is, those with an insufficient mass to affect the orbit of the planet doing the scattering.

[2] Note that equation (7) becomes inaccurate for Oort Clouds with semimajor axes approaching the tidal radius of the star (see fig. 7 of Weinberg, Shapiro & Wasserman 1987); that is, large-radius Oort Clouds may be more readily depleted than assumed.

However, this only restricts the applicability to the scattering of objects that are an order of magnitude or so less in mass than the planet, which means that it can also apply to scattered planets (so long as they are small in mass in comparison with the planet doing the scattering).

To assess this applicability more quantitatively, consider two planets of mass M_1 and M_2 on circular coplanar orbits at a distance a that undergo scattering, leaving M_1 on an orbit with an apocentre at a and eccentricity e_1 and M_2 on an orbit with a pericentre at a and an eccentricity $e_2 \approx 1$. Conservation of angular momentum shows that

$$\frac{M_2}{M_1} = \frac{1-\sqrt{1-e_1}}{\sqrt{2}-1}, \tag{11}$$

which means that $M_2/M_1 < 2.4$, and so the planet that is scattered out cannot be significantly more massive than that which did the scattering, but can be comparable in mass. This means, for example, that Jupiter-mass planets at a large distance would require planets of Jupiter mass or greater orbiting close-in if the former are required to have been scattered out, though the close-in planet need not continue to exist after the scattering, since it could have collided with the star.

Equation (11) can also be used to estimate the eccentricity imparted to the inner planet in this process, since for small e_1, this reduces to $M_2/M_1 \approx 1.2e_1$. Thus, a rule of thumb is that the maximum eccentricity gained by M_1 is of the order of M_2/M_1 (unless M_2 is ejected in a single encounter that placed it significantly above the escape velocity from the star's gravitational potential). This explains the magnitude of the eccentricity imparted to Jupiter on scattering Neptune and Uranus into the Kuiper belt in the instability proposed by Tsiganis et al. (2005), since $e_{\rm Jup} \sim M_{\rm Nep}/M_{\rm Jup}$.

3 APPLICATIONS TO SPECIFIC SYSTEM PARAMETERS

Here we consider what the planet mass versus semimajor axis parameter space looks like for four different system parameters. The primary aims of this section are to illustrate how this parameter space can be used to arrive at conclusions about the dynamics of a particular system, to corroborate the success of this framework at predicting outcomes by comparison with numerical simulations in the literature, and to introduce some potential outcomes to be explored further in Section 4.

3.1 Current Solar system

Having outlined the method for dividing the planet mass–semimajor axis parameter space into regions in which planets have different outcomes in Section 2, let us first consider the implications of the resulting parameter space for a system with parameters similar to that of the Solar system. That does not mean a system with planets like those in the Solar system (although such a system will be considered), rather a system orbiting a 1-$M_\odot$ star with an age of 4.5 Gyr in a local mass density of 0.1 $M_\odot$ pc^{-3} (and assuming planet densities of 1 g cm^{-3}), as plotted in Fig. 1.

Oort Cloud. The conclusions that can be reached from this figure about the formation of the Oort Cloud are well known. For example, T93 showed that the parameter space in which an Oort Cloud forms is quite restricted, and that those Oort Clouds that do form have a narrow range of semimajor axes ∼10 000 au. While this parameter space is inhabited by Uranus and Neptune in the Solar system, which should thus readily supply objects to the Oort Cloud (even accounting for the possibility that these planets may have started closer to the Sun; Tsiganis et al. 2005), it could be that Oort Clouds are relatively rare. Many simulations have confirmed these predictions regarding the ability of planets to implant objects in the Oort Cloud (e.g. Dones et al. 2004) while also showing further subtleties such as the ability of Jupiter and Saturn to place a small fraction of the objects they scatter into the Oort Cloud even if ejection is the predominant outcome in such encounters (Brasser, Duncan & Levison 2008). The time-scale predicted for the scattering process to occur is also borne out in numerical simulations. For example, compare the prediction of Fig. 1 that it should take 0.1–1 Gyr for Uranus and Neptune to implant material in the Oort Cloud with fig. 13 of Dones et al. (2015). The radius at which the Oort Cloud forms in the simulations also agrees with that predicted of ∼10 000 au, with some studies includingthe differentiation between inner and outer Oort Clouds (e.g. Lewis, Quinn & Kaib 2013; Brasser & Schwamb 2015). Inspection of Fig. 1 shows that Oort Clouds could form at smaller orbital radii, but that such an outcome requires both low-mass planets and a large system age; for example, if Neptune and Uranus were each of Earth mass, then the Oort Cloud would be at ∼1000 au, but would take ∼20 Gyr to form. Another way to achieve a small Oort Cloud on a shorter time-scale is to place the planetary system in a dense stellar environment (as discussed in Section 3.2).

Ejected. As noted in Brasser et al. (2008), many of the exoplanets known at that time will end up ejecting most of the material they encounter. The time-scale for these planets to eject material is usually relatively rapid, typically $\ll$10 Myr. That Jupiter is an efficient ejector of comets is common knowledge, given a basic understanding of cometary dynamics. That planets across a wide range of masses and semimajor axes far from their star also eject nearby material is also recognized by those studying planet formation (Goldreich, Lithwick & Sari 2004) and those studying cometary evolution [see e.g. the simulations of Higuchi, Kokubo & Mukai (2006) that confirm ejection as the dominant outcome for Jupiter-mass planets at 1–30 au and 0.1–10 Jupiter-mass planets at 5 au). However, the region of parameter space of planets for which ejection is the most likely outcome should be more widely acknowledged, since the presence of such planets in a system has a significant effect on the dynamics of scattered material. Any orbit that crosses such planets has a high probability of being ejected from the system, and so while material may pass back and forth between an orbit interior and exterior to a planet as it undergoes multiple scattering events, it is unlikely for material to pass from an orbit that is entirely interior to such a planet to one entirely outside the planet (and likewise from an exterior to interior orbit), unless there is a force acting on this material that changes the orbit faster than the scattering time-scale. Thus, any system known to have an eccentric Jupiter planet or a long-period giant planet (i.e. 5–10 per cent of stars) has an efficient ejector, and ejectors could be much more common, given that there is a large region of parameter space in which it cannot yet be known whether a system has an ejector (e.g. Saturn-mass planets at 10–30 au). We return to this in Section 4.2, since it has implications for comet-like populations. It is also the case that for circumbinary planets, the secondary star of the system would lie in the ejected regime, explaining why planets that are placed on to orbits that cross the stellar region end up being ejected from the system, rather than impacting one of the stars (Smullen, Kratter & Shannon 2016).

Accreted. More exoplanets are now known in the region in which the dominant outcome is accretion on to the planet; these are the hot Jupiter and super-Earth populations discussed in Section 2.1. Any material being scattered by such planets will end up being accreted

on to the planets on a relatively short time-scale, which, among other consequences, facilitates continued growth of these planets. That material could consist of leftover debris from the planet formation process (e.g. the late veneer thought to have been accreted by the Earth; Schlichting, Warren & Yin 2012), or debris that finds its way into this region at a later epoch (such as the near-Earth asteroids, Bottke et al. 2000)), and could include planetary embryos (e.g. Section 2.5). Thus, extra embryos do not tend to escape this region but are accreted on to existing planets (e.g. Ford & Rasio 2008; Petrovich, Tremaine & Rafikov 2014). Even if collisions between the embryos and the planets release a large mass of debris, this debris would eventually be reaccreted on to the planets, as would any escaping planetary moon. This is confirmed in numerical simulations of the dynamical evolution of giant impact debris, which find that debris from the Earth's Moon forming impact reaccretes on to the Earth on a time-scale of ∼15 Myr (Jackson & Wyatt 2012), and that it takes ∼0.3 Myr for debris released from an 18-$M_\oplus$ planet at 0.63 au to reaccrete on to that planet (Wyatt & Jackson 2016). These time-scales agree well with those predicted by equation (3), given that this calculation does not account for the non-axisymmetric geometry or multiplanet interactions involved in the simulations being compared to. The eventual fate of giant impact debris is discussed further in Section 4.1. The only way for a mass that finds itself in this region to avoid ending up on a planet is for it to end up on the star, or to get ground into dust that is removed by radiation pressure. This principle may go some way to explaining why these inner regions commonly retain a large mass in planets. Again, this is well known from simulations of terrestrial planet formation (e.g. Chambers 2001), but the region of parameter space to which this outcome applies as a fundamental principle should be more widely acknowledged, since it implies that planets interact differently with circumstellar material inside and outside the $v_{\rm esc} = v_{\rm k}$ line. Indeed, it is suggestive that the known exoplanet populations appear to be separated by this line, although the absence of ∼100 $M_\oplus$ planets in the ∼0.3 au region is more likely explained by the rapid growth and migration of such planets in interactions with the gas disc (Ida & Lin 2004; Mordasini, Alibert & Benz 2009). Some aspects of super-Earth formation are discussed further in Section 4.4.4.

Remaining. The conclusion that planets in the inner regions (≪5 au) accrete everything they encounter only applies to planets above a certain mass, since low-mass planets would not have had enough time to accrete all of the material they encounter. For a 4.5-Gyr system, this implies that primordial debris may be able to persist near Mars-mass planets at 4 au, or near more massive planets farther out. The same applies in the outer regions; for example, at the 700 au distance of the putative planet nine in the Solar system (Batygin & Brown 2016), even a 10-$M_\oplus$ planet would not have ejected planetesimals in its vicinity over 4.5 Gyr. However, particularly at small separations (but also farther out), mutual collisions amongst the debris need to be considered, since these would deplete this population at a rate which depends on the total mass of debris and the size of the largest object in the debris population, as well as the level of stirring (Wyatt et al. 2007b; Heng & Tremaine 2010). Thus, the outcomes shown in Fig. 1 are strictly only those that apply to low-mass debris populations, and it should be noted that for sufficiently massive debris populations, it may be possible to remove some of the debris expected to be *remaining* within the given time-scale by collisional grinding; collisional grinding may also allow debris to avoid the fate of being accreted on to the planet (e.g. Jackson & Wyatt 2012). This is considered further in Section 4.1 in application to giant impact debris.

3.2 Young Solar system formed in a cluster

Fig. 2 aims to recreate the conditions in the simulations of Brasser, Duncan & Levison (2006), which explored the consequence of the Sun spending the first 3 Myr of its life in a stellar cluster with a mean density 1.5×10^4 $M_\odot$ pc^{-3}, evidence for which may be present in the isotopic composition of minor Solar system bodies (Adams 2010). For this calculation, we used the equations of Section 2.4 assuming ρ_0 as the mean density. While the tide from a stellar cluster acts on a slightly different time-scale from that of a galactic disc, its dependence on the various parameters scales in the same way, and the change in the prefactor in equation (5) is <30 per cent and so is ignored for the purposes of this plot, given the much larger uncertainty in the mean density. Indeed, considerations of the birth environment of the Sun suggest that a mass density that is an order of magnitude lower may be more appropriate (Adams 2010), and more recent simulations have shown the need to include the effect of gas in the cluster (e.g. Brasser, Duncan & Levison 2007). Nevertheless, this plot illustrates the different possible outcomes that may be achieved by placing the planetary system in a dense environment. Apart from the younger age, which means that the planets have to be considerably more massive to have induced their respective outcome by 3 Myr, the main consequence of this scenario is that the higher mass density increases the importance of tides. This changes both the types of planets which can implant material in the Oort Cloud (equation 6) and the orbital radius of that Oort Cloud (equation 5). The region of parameter space in which planets can cause Oort Clouds is still relatively small but includes Saturn for the parameters chosen here. Such a scenario is often invoked to explain the origin of detached Kuiper belt objects like Sedna on wide orbits at 100–1000 au (e.g. Kaib & Quinn 2008), and indeed the putative planet nine (Batygin & Brown 2016). The simulations show that, for suitable cluster conditions, it is plausible that such objects can have formed in the inner regions of the Solar system and have been scattered out by interactions with the planets, whereupon they were detached from the planetary system by tides (Brasser et al. 2006). Some nearby stars were also likely born in dense clusters and so could have analogous populations of detached objects orbiting relatively close to their star, a possibility which is discussed in Sections 4.3.2 and 4.4.2. It is also possible that some of the Solar system's Oort Cloud was captured by the Sun's gravitational field after these objects were ejected following formation in the circumstellar discs of other stars in the Sun's birth cluster (Levison et al. 2010). Thus, another consequence of the scenario in which a star forms in a dense cluster is that some of the planetesimals that escape the system (i.e. those interacting with planets in the Ejected or Depleted Oort Cloud regions of Fig. 2) could end up in the Oort Clouds of other stars in the cluster.

3.3 Young A-type stars like HR 8799

Fig. 3 considers the parameter space of a nearby young A star, that is, a 40-Myr-old 2-$M_\odot$ star in an environment with local mass density 0.1 $M_\odot$ pc^{-3} and local stellar density 0.045 $M_\odot$ pc^{-3}. Note that stellar encounters dominate over Galactic tides for such a high-mass star, which has been accounted for by increasing the effective local mass density by a factor of 1.6 (see Appendix A), though this is of little consequence since there is no Oort Cloud region for these parameters. This is meant to be appropriate for systems like those currently being surveyed by direct imaging to search for planets orbiting young stars in nearby moving groups. Such surveys have been successful at discovering both directly

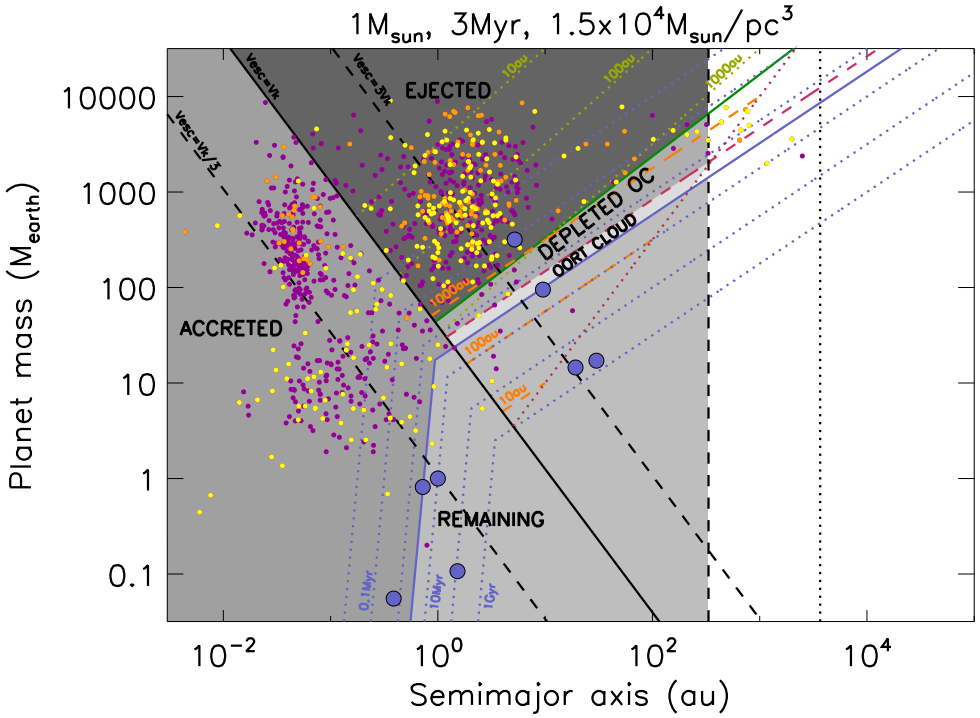

Figure 2. As for Fig. 1, but for a system orbiting a 1-$M_\odot$ star for 3 Myr of evolution in an environment with mass density 1.5×10^4 $M_\odot$ pc^{-3}. The vertical black dotted line is the tidal radius of the star for this local mass density (equation 9).

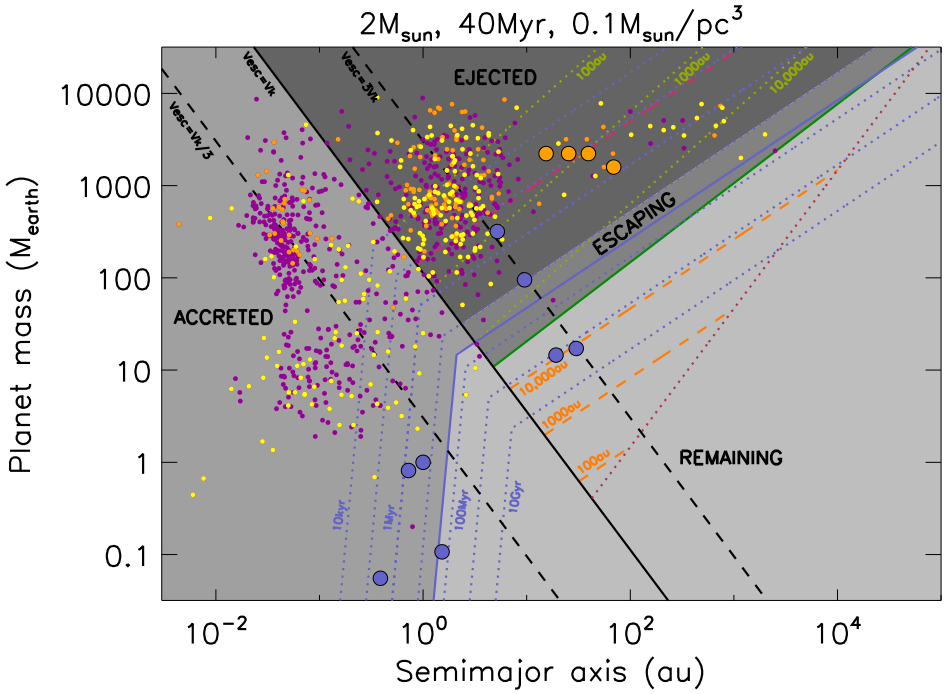

Figure 3. As for Fig. 1, but for a system orbiting a 2-$M_\odot$ star for 40 Myr of evolution in an environment with mass density 0.1 $M_\odot$ pc^{-3}. The four HR 8799 planets are shown as large orange dots at the locations of Goździewski & Migaszewski (2014) and masses of Konopacky et al. (2016).

imaged planets and debris discs, often in the same system. This type of system is epitomized by HR 8799, which is of comparable mass and age to those plotted, with four long-period giant planets of mass 3–9$M_{\rm Jup}$ imaged orbiting 12–60 au (Marois et al. 2010), and a debris disc extending both exterior (>90 au; Matthews et al. 2014b; Booth et al. 2016) and interior (<10 au; Su et al. 2009) to the planets.

Oort Cloud. Most of the differences between Figs 1 and 3 arise from the difference in system age; the difference in the stellar mass is not so important. One of the first things to note, as pointed out

by T93, is that young stars such as that plotted have not had time to form an Oort Cloud. That is, there is no Oort Cloud (or indeed depleted Oort Cloud) parameter space because the solid blue line lies entirely above the solid green line. Stars this massive can still form Oort Clouds by the end of their main-sequence lifetime (if they have suitable planets), and these would be at ∼10 000 au like that in the Solar system. However, Jura (2011) suggested that the Oort Clouds of A stars are, on average, less massive than that in the Solar system, based on the pollution signature of their white dwarf descendants. While their Oort Clouds could also have been depleted in the star's post-main-sequence evolution (Veras et al. 2011), if confirmed this could set constraints on the prevalence of planets in the relevant Oort Cloud region in these figures. As noted by T93, for stars that are massive enough ($>7\,M_{\odot}$), their main-sequence lifetime is not long enough for an Oort Cloud to form, although such stars also predominantly form in clusters, which may aid the rapid formation of a close-in Oort Cloud (e.g. Section 3.2).

Escaping. Otherwise, the parameter space looks similar in so far as the existence of ejected, accreted, and remaining regimes. However, the star's youth implies the existence of a population of escaping bodies, which was not discussed in Section 3.1. These are the objects which are still being scattered by planets in the cometary diffusion regime. While their ultimate fate is ejection from the system, many persist on highly eccentric orbits since the time-scale for that outcome is comparable to the age of the system. Such objects could be planets scattered from the planetary region or comet-like debris in a population analogous to the Kuiper belt's scattered disc. Veras, Crepp & Ford (2009) predicted a population of escaping planets that may be detectable around young stars scattered out during planetary system instabilities, while the scattered disc in the Solar system is (to some extent) a remnant of an escaping population which would have been much more massive at earlier times [e.g. equation (1) of Booth et al. (2009) shows that the characteristic time-scale for Uranus and Neptune to deplete the scattered disc is ∼280 Myr]. These populations are discussed further in Sections 4.3.1 and 4.4.1.

Ejected. Similar to the conclusions in Section 3.1, the population of known eccentric Jupiters and long-period giant planets would put material encountering them on to unbound orbits very rapidly. For example, the blue dotted lines show that the HR 8799 planets have diffusion times that are $\ll$1 Myr, and so would have long since removed any nearby planets and depleted any scattered disc by ejection. This means that the outer debris disc in HR 8799 cannot be composed of material currently being scattered by the known planets; rather this debris has only managed to survive this long because it is not encountering those planets, and so is a population more analogous to the classical Kuiper belt. Similar reasoning shows that the planet-like object Fomalhaut-b found at 130 au from its 440-Myr-old A star host Fomalhaut (Kalas et al. 2013) cannot be Jupiter in mass, unless it has been put on this orbit very recently. This was shown in numerical simulations (Beust et al. 2014; Tamayo 2014) but is implied from Fig. 3, since the diffusion time is ∼40 Myr at that distance and so the time-scale for the disruption of the narrow debris ring it traverses must be much shorter than this (assuming that the orbit of the planet brings it close enough to the debris for scattering to ensue), which, in turn, is clearly shorter than the age of the system. If, instead, Fomalhaut-b was a low-mass scattered disc object (e.g. closer to the proposal of Lawler, Greenstreet & Gladman 2015), the planet which scattered it on to such an eccentric orbit could be predicted to lie close to the line for which ejection takes 440 Myr (unless the object was only scattered recently); for example, equation (2) shows that such a planet at 32 au (the mean of the distribution of possible values for the pericentre of Fomalhaut-b's orbit, Kalas et al. 2013) would be $\sim 30\,M_{\oplus}$.

Remaining. The above reasoning does not preclude that the debris beyond 90 au from HR 8799 is in fact still interacting with unseen planets, since planets in that region that are in the *remaining* regime would not have had time yet to eject the debris in their vicinity. Fig. 3 shows that the diffusion time for planets in this region can be longer than the age of the system, even for planets up to Saturn in mass. The existence of such a planet could help to explain why the debris distribution extends from ∼145 au to beyond 400 au (Booth et al. 2016), since a planet orbiting close to the inner edge could have excited eccentricities in the debris population, creating an exterior scattered disc, an idea which is explored further in Section 4.3.1. Such a planet would need to be massive enough to stir the disc over the system age, but not so massive that it has ejected the majority of the debris, implying a roughly Saturn mass planet, although a comparison of the debris distribution with numerical simulations is needed for a more accurate determination. Note, however, that there is no requirement to invoke such a planet in this system, since the disc's breadth may alternatively be explained by an initially broad Kuiper belt.

Exocomets. IR observations indicate the presence of dust at ∼9 au, which is interior to the known planets of HR 8799 (Su et al. 2009). This is far enough from the star (and the planets) that it is compatible with an origin in the steady-state grinding of a planetesimal belt at that location analogous to the Solar system's asteroid belt (Wyatt et al. 2007a; Contro et al. 2015). In this paper, we consider an alternative explanation, which is that the hot dust is fed by comets scattered into the inner regions from the planetesimal belt beyond 90 au. While all four of the known HR 8799 planets lie deep in the *ejected* region, seemingly presenting a formidable barrier for any exocomets to cross, comets must still undergo many scatterings before ejection, some of which will have passed them inward. Thus, at any given time, there should be a population of objects residing in the inner regions that were scattered in from the outer disc. However, the short time-scale to achieve the ultimate fate of ejection (∼0.1 Myr) means that HR 8799's comet population is expected to be relatively small (at least compared to what it would be if the planets were lower in mass), and so may be unlikely to be the origin of its hot dust. Nevertheless, other systems may have architectures that are more suited to replenishing hot dust from exocometary populations, which are discussed further in Section 4.2.

3.4 Planets around low-mass stars

The discovery of three Earth-sized planets orbiting the M8 brown dwarf TRAPPIST-1 emphasizes that planetary systems are present around stars of all masses (Gillon et al. 2016). While the stellar mass made a little difference to the scattering outcomes for the stellar parameters considered in Figs 1 and 3, the mass of TRAPPIST-1 is just $0.08\,M_{\odot}$, which causes its scattering outcomes shown in Fig. 4 to be shifted substantially relative to their location in Fig. 1. While the three known TRAPPIST-1 planets would be expected to accrete most of the material they encounter, this is true for a smaller region of parameter space than for higher mass stars (although note that this is also a heavily populated part of parameter space; Winn & Fabrycky 2015). The most notable consequence of the star's low mass is the relative ease with which planets can eject objects which encounter them. The larger ejected regime makes it harder for a low-mass star to build up a planetary core that is capable of runaway accretion of gas (see also Payne & Lodato 2007), and means that even Earth-like planets can present a barrier that prevents comets

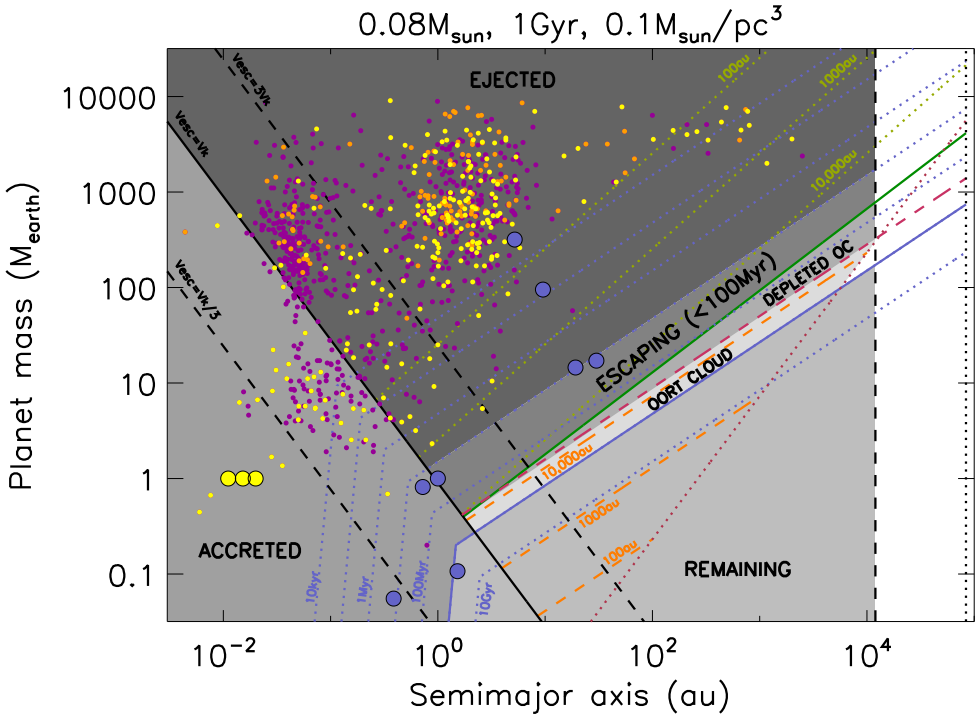

Figure 4. As for Fig. 1, but for a system orbiting a 0.08-M$_\odot$ star for 1 Gyr of evolution in an environment with mass density 0.1 M$_\odot$ pc^{-3}. The three planets found around TRAPPIST-1 are shown as large yellow dots (Gillon et al. 2016).

from reaching the inner regions of a system. Oort Clouds can still form, slightly within 10 000 au, and could be fed by scattering from planets as low in mass as the Earth at 5 au.

4 HOW TO MAXIMIZE DESIRED OUTCOMES

The interpretation of observations of planets or debris around nearby stars is usually hampered by the fact that we have only incomplete (if any) information about the rest of the planetary system. This leads to the necessity to consider the dynamics in a range of hypothetical systems to see if a plausible explanation for the observations can be found. Naturally, this requires consideration of an impossibly wide range of parameter space, and there is often no guarantee that any given plausible explanation is a unique explanation. Here we consider a number of different possible scattering outcomes that may be (or may have been) observed. On the basis that the first systems detected with a given outcome are likely to be those which nature has provided the most favourable planetary systems for achieving that outcome, here we focus on determining the architectures of the planetary system that would maximize the chance of observing the different outcomes. For the most part, we are not concerned with how such a system might form, so this does not mean that such systems are a plausible outcome of planet formation processes for which other considerations are involved. However, if the required outcome cannot be reproduced with the most favourable planetary system architecture imaginable, then it is likely that the proposed mechanism cannot be invoked to explain the observation under consideration. We also consider what constraints might be placed on a system's planets based on the planetary system architectures which cannot produce a given outcome.

4.1 Giant impact debris

The final stage in the formation of the terrestrial planets is thought to have been characterized by multiple giant impacts as the large number of embryos formed is whittled down by merging collisions to the few terrestrial planets seen today (Chambers 2001; Kenyon & Bromley 2006). Debris released in such impacts may persist in the system at levels that are detectable due to the dust created in its mutual collisions for tens of Myr (Jackson & Wyatt 2012; Genda, Kobayashi & Kokubo 2015). While the collisional evolution of giant impact debris must be accounted for when considering its detectability (e.g. Wyatt & Jackson 2016), Fig. 1 can already be used to reach some conclusions about the types of terrestrial planets which are most favourable for producing detectable debris. For example, this shows that the planets that make debris that can persist in the face of reaccretion on to the planet for >10 Myr are found at >1 au (see equation 3), with relatively little dependence on the planet mass (because while higher mass planets have a larger collision cross-section, their higher escape velocity means that their debris extends across a larger volume). However, the planets cannot be too far from the star because planets at large distances have an escape velocity that is higher than their Keplerian orbital velocity (e.g. $\gg$7 au, equation 1), which means that most of the debris that is created is quickly placed on to unbound orbits. Furthermore, the planets cannot be too low in mass, since larger quantities of debris are likely to be created in collisions with more massive planets (with the caveat that if the planet has an atmosphere, then this might prevent the escape of debris in impacts, Inamdar & Schlichting 2016), which is thus likely to be more readily detectable. These considerations suggest that there is a sweet spot in the planet mass–semimajor axis parameter space at which giant impact debris is most likely to be detected (in that it will be both bright and

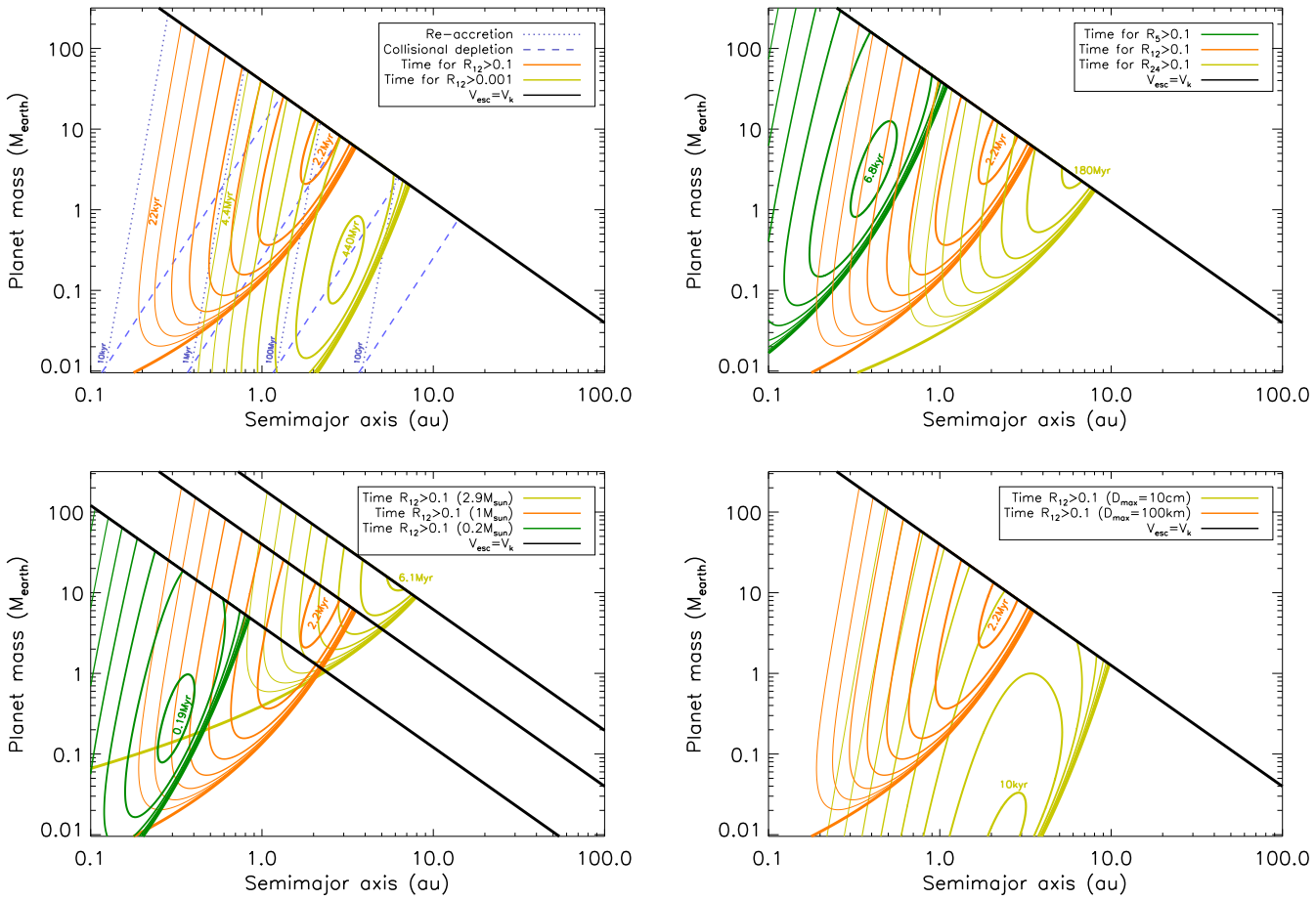

Figure 5. Planet mass versus semimajor axis parameter space showing time-scales relevant for the evolution of giant impact debris originating from such planets. Unless stated otherwise, it is assumed that the planet is orbiting a Sun-like star (1 $M_\odot$, 1 $L_\odot$, 5780 K), and the escaping debris has $f_{\rm esc} = 0.05$, $D_{\rm max} = 100$ km, $Q_{\rm D}^\star = 10^5$ J kg^{-1}. Debris is not considered above the black line for which the planet's escape velocity equals its Keplerian velocity. The blue dotted lines on the top left-hand panel show the time-scale for reaccretion on to the planet (equation 3), while that for depletion in mutual collisions is shown with blue dashed lines (equation 16); the annotation is placed where these two time-scales are equal. The other lines are contours on which the time-scale is the same for the thermal emission from the debris to remain above a given fractional excess level at a given wavelength, which for most panels means a fractional excess of 0.1 at a wavelength of 12 μm. The contours for each set of parameters are shown with a different colour, as indicated in the legend for each panel. In each case, the maximum time is indicated in the figure with the same colour as the contours, with the contours drawn at logarithmic intervals of 0.01, 0.019, 0.036, 0.069, 0.13, 0.25, 0.47, and 0.9 times this maximum time. The thick coloured lines show the planet mass below which the debris is never detectable at the relevant level (equation 14). The top left-hand panel shows the effect of changing R_λ, the top right-hand panel shows the effect of changing λ, the bottom left-hand panel shows the effect of changing stellar mass (assuming a 2.9-$M_\odot$, 54-$L_\odot$, 9500-K star and a 0.21-$M_\odot$, 0.011-$L_\odot$, 3250-K star), and the bottom right-hand panel shows the effect of changing $D_{\rm max}$, as noted in the legend.

long-lived). This would be expected to be for planets of a few $M_\oplus$ at a few au. The sweet spot is quantified in Sections 4.1.1 and 4.1.2, and its implications considered in Section 4.1.3.

4.1.1 Characterizing the sweet spot

To quantify this sweet spot, including a consideration of the effect of collisions amongst the debris population, Fig. 5 focusses on the planets for which giant impact debris is expected to be potentially detectable. For this figure, it was assumed that a giant impact puts into the circumstellar orbit a fraction $f_{\rm esc} = 0.05$ of the mass of the planet, so that the initial mass of debris

$$M_{\rm d0} = f_{\rm esc} M_{\rm p}; \tag{12}$$

see Table 2 for a summary of the additional parameters used in this section. This debris is assumed to have a power-law size distribution with index −3.5 (i.e. $dn/dD \propto D^{-3.5}$) extending from a diameter of $D_{\rm max} = 100$ km down to the radiation pressure blow-out limit (see equation 14 of Wyatt 2008), where the debris is assumed to have the same density as the planet ($\rho_{\rm p}$).

Further assuming that the dust acts like a blackbody, this means that the debris has a temperature

$$T = 278.3 L_\star^{1/4} a_{\rm p}^{-1/2}, \tag{13}$$

and starts with a fractional luminosity that is given in equation (15) of Wyatt (2008), from which the thermal emission at a wavelength λ can be derived using equation (10) of that paper. The thick coloured lines in Fig. 5 show the planets for which their giant impact debris starts out with thermal emission at the given level of fractional excess R_λ (i.e. the disc flux divided by the stellar flux at a wavelength λ), which are given by

$$M_{\rm p} = 2.4 \times 10^{10} T_\star^{-4} L_\star^{3/2} M_\star^{-1/2} \left[\frac{B_\nu(\lambda, T_\star)}{B_\nu(\lambda, T)}\right] D_{\rm max}^{1/2} \rho_{\rm p}^{-1/2} f_{\rm esc}^{-1} R_\lambda, \tag{14}$$

Table 2. Summary of parameters introduced in Section 4.1.

Parameter	Symbol	Units
Stellar temperature	$T_\star$	K
Fraction of mass escaping as debris	$f_{\rm esc}$	Dimensionless
Initial mass of debris	$M_{\rm d0}$	$M_\oplus$
Instantaneous mass of debris	$M_{\rm d}$	$M_\oplus$
Diameter of largest debris fragment	$D_{\rm max}$	km
Debris temperature	T	K
Observing wavelength	λ	μm
Planck function	B_ν	Jy sr^{-1}
Fractional excess	R_λ	Dimensionless
Dispersal threshold	$Q_{\rm D}^\star$	J kg^{-1}
Initial collisional lifetime of debris	$t_{\rm c0}$	Gyr
Instantaneous collisional lifetime	$t_{\rm c}$	Gyr
Reaccretion time-scale	$t_{\rm acc}$	Gyr
Fraction of debris mass reaccreted	$f_{\rm acc}$	Dimensionless
Ratio of $t_{\rm acc}/t_{\rm c0}$	η	Dimensionless
Time debris mass is above $M_{\rm d}$	$t_{(>M_{\rm d})}$	Gyr
Time fractional excess is above R_{12}	$t_{(>R_{12})}$	Gyr

where $L_\star$ has units of solar luminosity, B_ν is the Planck function at the given wavelength and temperature, and $T_\star$ is the temperature of the stellar emission. Planets must be above these lines for their giant impact generated debris to be detectable at the given level.

Assuming that the debris has a dispersal threshold $Q_{\rm D}^\star = 10^5$ J kg^{-1}, which is independent of size, the time-scale for mutual collisions amongst the debris population to deplete the debris is given by equation (16) of Wyatt (2008) with the further assumption that the width of the torus and its stirring are set by the planet's escape velocity. This gives a collisional lifetime of

$$t_{\rm c} = 6.4\times10^{-12} M_\star^{-1} a_{\rm p}^4 M_{\rm p}^{-2/9} \rho_{\rm p}^{-1/9} D_{\rm max} {Q_{\rm D}^\star}^{5/6} M_{\rm d}^{-1} \quad (15)$$

in Gyr, where $M_{\rm d}$ is the total mass of debris at that time in $M_\oplus$. This collision lifetime has a very strong dependence on the distance from the star, which goes some way to explaining why there are so few Vulcanoid asteroids in the Solar system (Steffl et al. 2013), since these are otherwise long-term dynamically stable (Evans & Tabachnik 1999), but would have been eroded by mutual collisions over the age of the Solar system (Stern & Durda 2000).

Equation (15) can be rearranged to find that the planet mass that results in giant impact debris that starts out with a collisional lifetime $t_{\rm c0}$ in Gyr is

$$M_{\rm p} = 6.9\times10^{-10} M_\star^{-9/11} a_{\rm p}^{36/11} \rho_{\rm p}^{-1/11} D_{\rm max}^{9/11} {Q_{\rm D}^\star}^{15/22} f_{\rm esc}^{-9/11} t_{\rm c0}^{-9/11}, \quad (16)$$

which is plotted in the top left-hand panel of Fig. 5 with dashed blue lines, along with the dotted blue lines which give the planets that result in a given reaccretion time-scale (i.e. the same as those in Fig. 1).

The eventual fate of the mass of debris depends on $\eta = t_{\rm acc}/t_{\rm c0}$, which is the ratio of the time-scale on which the debris is reaccreted on to the planet to that on which its initial mass is ground into dust (which is subsequently removed by radiation pressure). Rearranging equation (3) shows that reaccretion on to the planet takes place on a time-scale

$$t_{\rm acc} = 0.01 M_\star^{-1} a_{\rm p}^4 \rho_{\rm p}^{5/6} M_{\rm p}^{-1/3}, \quad (17)$$

while $t_{\rm c0}$ is calculated using equation (15) with $M_{\rm d} = M_{\rm d0}$, giving

$$\eta = 1.6\times10^9 \rho_{\rm p}^{17/18} M_{\rm p}^{8/9} D_{\rm max}^{-1} {Q_{\rm D}^\star}^{-5/6} f_{\rm esc}. \quad (18)$$

With these two loss mechanisms, the rate of debris mass-loss is

$$\dot{M}_{\rm d} = -M_{\rm d}/t_{\rm acc} - M_{\rm d}/t_{\rm c} = -M_{\rm d}/t_{\rm acc} - M_{\rm d}^2/(M_{\rm d0} t_{\rm c0}), \quad (19)$$

which can be solved to give

$$M_{\rm d} = M_{\rm d0}[\exp(t/t_{\rm acc}) + \eta(\exp(t/t_{\rm acc}) - 1)]^{-1}, \quad (20)$$

as well as showing that the fraction of mass that is eventually accreted is

$$f_{\rm acc} = \eta^{-1} \ln(1+\eta). \quad (21)$$

Equation (20) can be rearranged to give the time for which the debris has a mass above a given level:

$$t_{(>M_{\rm d})} = t_{\rm acc} \ln\left(\frac{\eta + M_{\rm d0}/M_{\rm d}}{\eta + 1}\right). \quad (22)$$

This is used in Fig. 5 to work out, for each planet mass and semimajor axis, the length of time the giant impact debris from that planet would have a fractional excess above a given level R_λ (i.e. $t_{(>R_\lambda)}$), by using equation (12) for $M_{\rm d0}$, and using for $M_{\rm d}$ the mass required to give this fractional excess (which is $f_{\rm esc}$ times the right-hand side of equation 14). Lines of constant $t_{(>R_\lambda)}$ are shown in Fig. 5 as the thinner solid lines with the different colours corresponding to different combinations of model parameters or detection thresholds. This is one way to visualize the sweet spot, since for a uniform frequency of giant impacts per logarithmic bin of planet mass and semimajor axis, debris would be expected to be seen at a higher incidence in regions of highest $t_{(>R_\lambda)}$.

For Fig. 5, we have not considered debris above the $v_{\rm esc} = v_{\rm k}$ line, which is shown in black. However, it is, in principle, possible to take this into account by working out the fraction of debris that is placed on to bound orbits in this regime, and to use as the lifetime of this debris that from cometary diffusion.

4.1.2 *Parameter dependence of sweet spot*

The shape of the sweet spot in Fig. 5 is close to that predicted in Section 4.1. Indeed, the lowest contours (i.e. those for which the debris does not last long above the detectable level) are bounded at the top right-hand edge and bottom right-hand edge by equations (1) and (14), respectively, while the left-hand edge is near the corresponding isochrone for reaccretion on to the planet (i.e. the dotted line given by equation 3). It may seem counter-intuitive that the time-scale for the debris to remain above the given R_{12} level can be set by the reaccretion time-scale in this regime, since the initial collisional depletion time-scale (i.e. the dashed line given by equation 16) is shorter than that for reaccretion. However, the collision time-scale $t_{\rm c}$ gets longer as the debris mass is depleted, leading to that mass dropping inversely with age, which is much slower than the exponential depletion in mass caused by reaccretion (albeit on a longer time-scale). Thus, the relevant time-scale depends on whether a large or small fraction of the initial debris mass needs to be removed to drop below the detection threshold (in which case reaccretion or collisional depletion, respectively, are dominant). This means that the contours at larger semimajor axes do not follow the reaccretion time-scale but, instead, reach a maximum time for the debris to remain above the detection threshold that is set by collisional depletion. It is interesting to note that it is not necessarily the most massive planets for which the debris is detectable the longest (i.e. the maximum time does not occur on the $v_{\rm esc} = v_{\rm k}$ line). This arises because collisional depletion is faster for debris from higher mass planets (see equation 15), which is because

mutual collisions amongst the debris occur at higher velocities (as well as the debris being dispersed into a larger volume).

With this understanding of the origin of the sweet spot, the dependence of its shape on the different parameters can also be readily understood. For example, the top left-hand panel of Fig. 5 shows two values of R_{12}. The $R_{12} > 0.1$ threshold is achieved for tens of thousands of stars by photometric instruments such as *WISE* (e.g. Kennedy & Wyatt 2013), while the $R_{12} > 10^{-3}$ threshold is the goal of cutting-edge nulling interferometry techniques that may be achieved on bright stars (e.g. Defrère et al. 2016). In the former case, we find that the sweet spot is for planets more massive and farther from the star than the Earth, for which the debris remains detectable for 1–2 Myr. For the lower detection threshold, the debris from lower mass (i.e. Mars-mass) planets becomes accessible, with planets at ∼3 au having debris that remains detectable for 200–400 Myr. This can be understood from the lower detection threshold given by equation (14), which means that lower masses of debris are detectable, which, in turn, allows the debris from planets at larger orbital radii to be detectable, whereupon the longer evolutionary time-scales mean that it can remain so for longer periods.

For a similar reason, there is also a dependence on the wavelength of observation, which sets the lower envelope of the sweet spot through equation (14), and, in particular, through the ratio of Planck functions in the square brackets. This ratio is minimized when the wavelength is long enough for the dust to be emitting in the Rayleigh–Jeans limit, or equivalently for debris that is close enough to the star for this to be the case, at which point the ratio scales $\propto T_\star/T \propto T_\star L_\star^{-1/4} a_{\rm p}^{1/2}$. This is true for the closest planets at ∼0.1 au in the top left-hand panel of Fig. 5. Thus, it can be expected that the $R_{24} > 0.1$ line would be similar to that of R_{12} at small radii (where it would scale $\propto a_{\rm p}^{1/2}$) but would depart from this scaling and turn up towards higher planet masses at orbital radii that are farther out than the turn-up for R_{12}. This is confirmed in the top right-hand panel of Fig. 5, and means that giant impacts should be more readily detected at longer wavelengths, with the caveat that observations at longer wavelengths do not necessarily have the same sensitivity to fractional excess, and/or it may be harder to distinguish giant impact debris from steady-state grinding of exo-Kuiper belts at longer wavelengths. Conversely, at shorter wavelengths like 5 μm, detected impact debris would be expected to be closer to the star, and to be seen relatively infrequently, given the shorter duration of detectability.

The properties of the star also affect the location of the sweet spot. The lifetimes have a dependence on the stellar mass through equations (1), (3), and (16). However, the strongest effect on the sweet spot is again through the lower detection threshold limit in equation (14), which scales $\propto T_\star^{-3} L_\star^{5/4} M_\star^{-1/2}$ for the Rayleigh–Jeans limit discussed above. This means that the detection threshold for giant impacts around an A0V star in this limit is an order of magnitude higher than those plotted in the top left-hand panel of Fig. 5. However, the bottom left-hand panel of Fig. 5 shows that this does not necessarily mean that giant impact debris is less readily detected around higher mass stars because the debris is also hotter around a higher luminosity star, which causes the turn-up in the lower limit discussed in the previous paragraph to occur at larger radii. Overall, the bottom left-hand panel of Fig. 5 shows that giant impact debris around higher mass stars is seen out to larger radii, where it lasts slightly longer and requires a higher mass planet progenitor than a Sun-like star. Conversely, giant impact debris is detectable from planets orbiting lower mass stars, even for Mars-mass planets, but only if they are close-in (<0.5 au).

Some of the parameters in the calculation are quite uncertain, such as the largest planetesimal size $D_{\rm max}$ and the dispersal threshold $Q_{\rm D}^\star$. It must also be recognized that the dispersal threshold is known to be dependent on planetesimal size, which results in a debris size distribution that is more involved than that assumed here (e.g. Wyatt, Clarke & Booth 2011). Nevertheless, the assumptions used here provide a self-consistent and transparent model that also provides a reasonable approximation to the evolution of mass and debris luminosity. This means that the dispersal threshold is some kind of average of the size distribution and will not be discussed further, except to note that more accurate calculations can be done to explore this issue but will not affect the qualitative results presented here.

The largest planetesimal size is, however, an important parameter. For example, if most of the debris mass was vaporized and subsequently condensed into 10-cm-sized grains (Johnson & Melosh 2012), this would result in $D_{\rm max}$ being reduced by six orders of magnitude. The lower envelope of the sweet spot would be reduced by three orders of magnitude (equation 14), making the aftermath of impacts involving small mass planets detectable (see the bottom right-hand panel of Fig. 5). However, the collisional lifetime would also be reduced by six orders of magnitude, meaning that the debris would be short-lived at detectable levels, though again would be most readily detected at large orbital radii where collisional depletion times are longest. Conversely, if most of the debris mass was placed into larger objects, the giant impacts would need to involve higher mass planets to create detectable debris, but that debris would be detectable for longer.

4.1.3 Implications of the sweet spot

Having outlined the region in which giant impact debris lasts longest, the implication is that this should be where the first giant impact debris is detected. If not, this could imply that such planets do not exist, or that they do not suffer giant impacts if they do. One of the clearest examples of a star with giant impact debris is ∼20 Myr old HD 172555, with dust at 5.8 au from this A5V star (see Table 3; Lisse et al. 2009; Smith, Wyatt & Haniff 2012). A giant impact origin for the dust is inferred from its silica composition and abundance of submicron-sized grains. Taking the model at face value, given that the parameters of this star are closest to that of the 2.9-$M_\odot$ star in the bottom left-hand panel of Fig. 5, the detection of debris at this radial location is consistent with expectations. In fact, Fig. 6 shows that the dust is slightly farther out than the nominal model would predict for this star, but this can be accounted for by reducing the largest debris fragment size (see the bottom right-hand panel of Fig. 5), or by recognizing that there is a contribution to the dust luminosity from grains expected to have been removed by radiation pressure. Thus, if this is giant impact debris, we predict the presence of a 3–10 $M_\oplus$ planet orbiting coincident with the debris at 5–6 au (though the parent planet could be less massive depending on model parameters). Several other young A-type stars have also been suggested to have giant impact debris at a similar location (see Table 3, e.g. 4.3 au for EF Cha, Rhee, Song & Zuckerman 2007; 4 au for η Tel, Smith et al. 2009a), again consistent with their expected location (Fig. 6). This could mean that planets in this region of parameter space are relatively common around A-type stars. Such planets are absent in the known exoplanet population (see, e.g. Fig. 1), but this is because they are below the detection threshold of radial velocity and transit surveys.

There are also several examples of proposed giant impact debris found much closer to the star (e.g. HD 23514 at 0.25 au, Rhee

Table 3. Proposed giant impact debris around ≤120 Myr stars with excess emission detected at 12 μm. Parameters are taken from the literature, except for the stellar mass which is that appropriate for the spectral type.

Star	Spectral type	$L_\star$	$M_\star$	$T_\star$	Dust location	Reference
η Tel	A0V	22 $L_\odot$	2.9 $M_\odot$	9506 K	4 au	Smith et al. (2009a)
HD 172555	A5V	9.5 $L_\odot$	2.0 $M_\odot$	8000 K	5.8 au	Lisse et al. (2009); Smith et al. (2012)
EF Cha	A9	10 $L_\odot$	1.7 $M_\odot$	7400 K	4.3 au	Rhee et al. (2007)
HD 113766	F3/F5	4.4 $L_\odot$	1.4 $M_\odot$	5878 K	1.8 au	Lisse et al. (2008)
HD 15407A	F5V	3.9 $L_\odot$	1.4 $M_\odot$	6500 K	0.6 au	Melis et al. (2010); Fujiwara et al. (2012)
HD 23514	F6V	2.8 $L_\odot$	1.3 $M_\odot$	6400 K	0.25 au	Rhee et al. (2008)
ID 8	G6V	0.8 $L_\odot$	0.9 $M_\odot$	5500 K	0.33 au	Meng et al. (2014)
TYC 8241 2652 1	K2	0.7 $L_\odot$	0.7 $M_\odot$	4950 K	0.4 au	Melis et al. (2012)

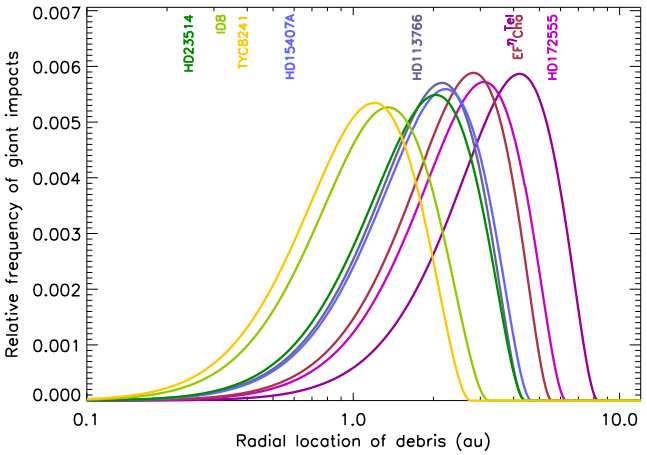

Figure 6. Distribution of radial locations of giant impact debris expected for the eight stars in Table 3; the number of expected detections scales with the area under the curve. Giant impacts are assumed to occur with an equal frequency per logarithmic bin of planet mass and semimajor axis, and it is assumed that the debris is characterized by $f_{\rm esc} = 0.05$, $D_{\rm max} = 100$ km, and $Q_{\rm D}^\star = 10^5$ J kg^{-1}, and is detected if $R_{12} > 0.1$. The different colours indicate the different stars, as shown in the annotation which is placed at the observed radial location of debris for this star.

et al. 2008; TYC 8241 2652 1 at 0.4 au, Melis et al. 2012; ID 8 at 0.33 au, Meng et al. 2014). It is notable that the stars with close-in debris are of later spectral type (F-, G-, and K-type stars) than those mentioned above with debris at a larger distance. Indeed, Table 3 shows a significant dependence of the radial location of the debris on spectral type. This trend was anticipated from the bottom left-hand panel of Fig. 5. However, since these stars are closest to the Sun in their properties, and the nominal model predicts that giant impact debris from planets at 1–3 au would be much longer-lived than that at ≪1 au, it is still surprising that more distant debris is not more prevalent in the population of known giant impact debris (see Fig. 6). There are three possible explanations for this: (i) The model parameters are wrong. (ii) The population in Table 3 is biased. (iii) There are a few giant impacts occurring with planets in the 1–3 au region.

(i) Increasing the largest debris fragment size is one way to preferentially detect debris at smaller radii (see the bottom right-hand panel of Fig. 5), but it is only possible to favour debris at a few tenths of an au with unrealistic (>1000 km) debris sizes. Favouring such small radii could be achieved by modifying the debris size distribution in other ways, to push up the detection threshold set by equation (14), but the upper envelope set by equation (1) means that this would inevitably require the debris to have been released from ∼100 $M_\oplus$ planets, which seems unlikely if such planets are primarily gaseous (e.g. Rogers 2015). It may also be possible to preferentially increase the duration of the detectability of close-in debris by including additional physics in the model. For example, one aspect that could increase the duration of the detectability of hot giant impact debris is its vaporization (and subsequent recondensation). The abundance of gas and optical depth effects during this early phase could make such debris persist at detectable levels much longer than predicted here, and such effects may be particularly relevant closer to the star (Jackson et al., in preparation).

(ii) Table 3 does not include all possible examples of giant impact debris, which should be a subset of the 12-μm-excess candidates found in surveys that searched all nearby stars (e.g. Kennedy & Wyatt 2013; Cotten & Song 2016). The problem is that an interpretation of such a set of candidates requires a careful consideration of whether the excesses come from giant impacts, from protoplanetary discs, or from a more distant exo-asteroid belt. We have concentrated here on the systems claimed in the literature as giant impact debris, but it could be that the more ambiguous interpretation of colder debris at >1 au has biased against including them in Table 3. To assess this, we considered the Kennedy & Wyatt (2013) sample of 12-μm excesses, excluding those thought to be protoplanetary or transition discs, those not confirmed to be <120 Myr, and those of earlier spectral type than F3. This leaves us with seven candidates, including HD 113766 and HD 15407, that are noted in Table 3, and five F3V–F8 stars with dust in the range of 1.3–2.7 au (HD 115371, HD 103703, HD 106389, HD 108857, HD 22680). If these are confirmed to have giant impact debris, then, given the expected distribution of dust locations for stars with similar stellar properties shown in Fig. 6, it is likely that this distribution is consistent with giant impacts that occur with an equal frequency in logarithmic bins of planet mass and semimajor axis. Note that the ∼Myr duration of detectability predicted by the model is also consistent with that estimated from giant impact debris from super-Earths in section 8 of Wyatt & Jackson (2016) from the fraction of 10–100 Myr stars with 12-μm excesses, which was in the range of 0.1–10 Myr. Given the implications discussed in (iii), a thorough analysis of potential giant impact debris to assess its origin is warranted.

(iii) The most interesting possibility is that the lack of giant impacts at 1–3 au arises from a lack of planets in this region. Like the A stars, the other detection techniques have yet to fully characterize the frequency of planets in this region. It is well known that super-Earth planets at ≪1 au are common, but the population farther out can only be assessed from the extrapolation of the population of planets closer in (see Winn & Fabrycky 2015). Thus, searches for giant impact debris potentially provide a way of assessing the ubiquity of planets in a region of interest to those studying habitable planets. While we cannot say that terrestrial planets cannot be commonly present at 1–3 au from Sun-like stars, if they were inferred to be less common than closer-in super-Earths, this would be in

contradiction to some extrapolations of that population (e.g. Traub 2012). For now, it is worth emphasizing that the underlying planet population should be imprinted in observations of the debris from giant impacts.

Another point to note from Table 3 is the absence of giant impact debris around late-type stars, such as M stars, since the bottom left-hand panel of Fig. 5 shows that even relatively low mass planets can result in giant impact debris that is at a detectable level. Moreover, transit studies have shown that planets are relatively common in exactly this region (Winn & Fabrycky 2015). Since the duration of detectability is only an order of magnitude lower than for Sun-like stars, in a region known to be abundant with planets, it would appear surprising that giant impact debris has yet to be detected around an M star. The explanation could be that the low luminosity of M stars means that they are inherently faint, and so it is not possible to detect debris down to levels of $R_{12} = 0.1$, except for the nearest stars. Alternatively, these planetary systems are born both stable and without extra embryos, such that giant impacts do not occur on the main sequence.

The above discussion has focused on young stars (within a few 100 Myr) and the possibility that embryos formed near the planet in question are the origin of giant impacts. However, another source of impactors is the exocomet population discussed in more detail in Section 4.2, which means that Gyr-old stars can also exhibit the giant impact phenomenon, and indeed the Kennedy & Wyatt (2013) sample of 12-μm-excess stars includes old stars such as BD +20307. Wetherill (1994) pointed out that increasing the comet scattering rate in the Solar system also increases the expected size of the largest impactor to have hit the Earth, from a 25-km body at the current epoch to one the size of Ceres in their simulation B. This points to the possibility that an increased comet population, as well as releasing dust through sublimation, mutual collisions, and disintegration, could result in a giant impact that releases large quantities of dust into the inner regions of a system. Lisse et al. (2012) suggested such a mechanism for the origin of hot dust in the η Corvi system, which is inferred to be at ∼3 au from this 1.4-Gyr-old F2V star. The spatial distribution of the hot dust provides one method to test this scenario because the geometry of collisional debris results in an asymmetry in the dust production location, which is enhanced at the point of impact for several 1000 orbits (Jackson et al. 2014). Observations of η Corvi are consistent with such an asymmetry, since while the dust temperature puts it at 3 au from the star (Lisse et al. 2012), a significant fraction of dust is seen at a closer projected separation of ∼0.7 au (Defrère et al. 2015; Kennedy et al. 2015). If this is the correct interpretation, then we have some constraints on the planet that was impacted, since a planet at 3 au which does not eject comets that approach it, but does accrete them, would be 0.1–10 $M_\oplus$. The number of known two-temperature debris discs is growing (Morales et al. 2011; Chen et al. 2014). Like η Corvi, the warmer inner components of these discs can often be confirmed to be spatially separated from the outer cooler components (Kennedy & Wyatt 2014), which may provide a source of impacts on to planets in the inner regions and so an explanation for the presence of the warm dust.

4.2 Exocomets

The flux of comets in the inner reaches of planetary systems is of particular interest because of its implications for the habitability of planets in the habitable zone (e.g. due to the delivery of water to the planets, and catastrophic impacts) and as a possible explanation for the Earth's Late Veneer (e.g. Morbidelli & Wood 2015). These comets may also replenish the dust discs known as exozodi that are seen within a few au of several stars from their excess near-IR to mid-IR emission (Absil et al. 2006; Smith, Wyatt & Haniff 2009b; Absil et al. 2013; Ertel et al. 2014; Mennesson et al. 2014). If they reach close enough to the star, or are favourably aligned to our line of sight, such comets may also show up in transit as they pass in front of the star (e.g. Jura 2005; Kiefer et al. 2014; Vanderburg et al. 2015; Boyajian et al. 2016).

In the Solar system, there are two main families of comets. The Ecliptic comets (such as the Jupiter-family comets) originate in the Kuiper belt, but following some perturbation they are dislodged from their initially stable orbit and start undergoing encounters with Neptune. Some of these scatterings pass the comets inwards through the Centaur region, where they come under the gravitational influence of scattering by the closer-in planets. Ultimately, most are ejected by Jupiter. However, some make it to the inner Solar system, where they appear as comets and disintegrate to replenish the dust in the zodiacal cloud (Nesvorný et al. 2010); a small fraction find a dynamical path to remain there as Encke-type comets (e.g. Levison et al. 2006). The long-period comets originate in the Oort Cloud and arrive in the inner Solar system once Galactic tides have sufficiently reduced the pericentres of their orbits. Planetary architectures that maximize the extrasolar analogues to these two comet families are discussed in Sections 4.2.1 and 4.2.2, respectively.

4.2.1 High cometary flux from exo-Kuiper belt

The question of how to maximize the cometary flux scattered in from an exo-Kuiper belt has been studied by several authors. For example, Bonsor & Wyatt (2012) showed how constraints on the Tisserand parameter give an indication of the types of chains of planets required to scatter comets in, which must be sufficiently tightly packed for scattered comets to reach a given proximity to the star or to start being scattered by the next planet further down the chain (see, e.g. their equation 3). This was followed up in Bonsor et al. (2012) by numerical simulations which quantified the comet influx from chains of planets, the conclusion of which was that comet influx is necessarily rather small. Bonsor, Raymond & Augereau (2013) and Bonsor et al. (2014) considered ways to increase the comet influx by allowing the outer planet in the chain to be scattered into, or to migrate into, the Kuiper belt to replenish the cometary population. Consideration of Fig. 1 shows that there are three main requirements in the design of a planetary system to maximize the comet influx. In addition to requiring a chain of closely separated planets, the following requirements also need to be fulfilled:

(1) *No ejector*. The most important requirement was raised in Section 3.1, which is that if there is a planet in the chain that is in the *ejected* region, then the comets may never make it into the inner system (or if they do, they do not remain there for very long) but, instead, are ejected from the system. This explains why Raymond & Bonsor (2014) concluded that the presence of a Jupiter-mass planet at >15 au is inconsistent with a scattering origin for the exozodiacal dust of Vega. It also explains why the Horner & Jones (2009) simulations in which they considered how the impact rate on the Earth from Centaurs (i.e. objects scattered in from the Kuiper belt) changes as the mass of Jupiter is changed. They found that the impact rate is maximized when the mass of Jupiter is close to that of Saturn. The increase in impact rate as Jupiter's mass is decreased is readily understandable from the arguments above because Jupiter is in the *ejected* region, and so decreasing its mass

reduces its ability to eject comets (or rather they survive longer and so a greater fraction reach the inner Solar system). The decrease in comet flux as Jupiter's mass is reduced below the Saturn mass arises because Saturn is also in the *ejected* region, and so can eject all of the comets that pass by the radius of its orbit, but only so long as there is no massive planet interior to its orbit that scatters comets away from Saturn's orbit on a shorter time-scale than that which Saturn ejects them. The conclusion that a large exocomet population is incompatible with a system with an ejector planet seems contradictory to the abundance of exocomets seen towards the star β Pic as falling evaporating bodies (FEBs; e.g. Kiefer et al. 2014), since this system is known to host the $9M_{\rm jup}$ planet β Pic-b orbiting at 9 au (Lagrange et al. 2010). However, the favoured model for the dynamical origin of the FEBs is in a mean motion resonance that is interior to β Pic-b (Beust & Morbidelli 2000); that is, the exocomets are not required to have crossed the planet's orbit in this system. The edge-on orientation and youth of the β Pic system may also play a role in the detectability of this phenomenon.

(2) *Inward torque.* Another requirement on the chain of planets is that the comets have to be passed inwards. If not, they will end up undergoing the cometary diffusion described by T93, which either implants them in the Oort Cloud or ejects them. The resulting requirement on the planets is beyond the scope of this paper, but a general comment is that during the early stages of scattering, the particles tend to be scattered both interior and exterior to the planet. The requirement for an interior planet to start dominating the scattering process is thus likely to be when the time-scale for scattering by that inner planet is shorter than the time-scale for scattering by the planet in question. Since these time-scales will scale with orbital period, the expectation would be that the tipping point would be close to flat in mass with distance. (This is the reason the Horner & Jones (2009) simulations found that Jupiter should be comparable in mass to Saturn for its ability to scatter comets inwards to be comparable with the ability of Saturn to eject comets.) However, the exact mass distribution required to pass comets inwards also depends on the separation between the planets. Bonsor et al. (2013) and Raymond & Bonsor (2014) show that decreasing the planet separation increases the rate at which particles are scattered inwards, although they also found that there are specific configurations related to resonances that can increase the efficiency of inward scattering; if too closely packed, the planetary system may also become unstable (e.g. Faber & Quillen 2007). Nevertheless, it is clear that an inward flow requires that planet mass does not increase too strongly with radius. Indeed, Raymond & Bonsor (2014) show that chains of planets with decreasing planet mass as a function of distance scatter planetesimals inward more efficiently than those with increasing mass, though note that all of their simulations included a planet in the ejection region.

(3) *Replenishment.* Finally, another requirement is for the population of comets undergoing scattering to be replenished. The problem is that objects on unstable orbits tend to undergo scattering and are consequently removed relatively quickly from the system, on a time-scale $t_{\rm sca}$, while objects on stable orbits can remain unperturbed over Gyr time-scales. Defining M_0 to be the initial mass of the comet belt, another way of stating the above problem is that it is possible only to get comet mass influx rates approaching $M_0/t_\star$ early on in the evolution (i.e. for $t_\star \ll t_{\rm sca}$), as shown, for example, in the simulations of Bonsor et al. (2012). This is why Bonsor et al. (2014) invoked outward migration of the outer planet because as long as this can be sustained over $t_\star$ time-scales, the resulting migration of its unstable resonance overlap region causes objects on previously long-term stable orbits to end up in an unstable region where they could undergo scattering with the planet. Alternatively, Bonsor et al. (2013) invoked a dynamical instability which was triggered late on, starting at a time $t_\star \gg t_{\rm sca}$, which allowed comet influx rates of $M_0/t_{\rm sca}$ that are significantly in excess of $M_0/t_\star$ but only for short periods of time. Another mechanism proposed by Faramaz et al. (in preparation) involves long-time-scale diffusion in resonances (e.g. Murray & Holman 1997), which can allow large influx rates on Gyr time-scales but requires the majority of the belt to be near resonances to achieve influx rates of $M_0/t_\star$. Here we propose that a planet (or planets) embedded within a planetesimal belt could place those planetesimals on to orbits that cross an interior planetary system where they may undergo further scattering. This is similar to the suggestion that dwarf planets embedded in the Kuiper belt excite eccentricities in the Kuiper belt population, which could place them on unstable orbits over a time-scale comparable to the age of the Solar system (Muñoz-Gutiérrez et al. 2015). It is also similar to the embedded planets scenario proposed in Section 3.3 to explain the broad disc of HR 8799, since as well as scattering debris out, some will also get scattered in where it can interact with an inner planetary system potentially ending up on comet-like orbits. For a system of given age, the maximum rate of comet influx ($M_0/t_\star$) is likely to arise for an embedded planet which has a time-scale for depleting the disc of the order of the age of the system (since more massive planets would have depleted the disc long ago, while less massive planets would scatter material in too slowly). For HR 8799-like parameters, this would argue for a planet at 100 au that is around Saturn mass, similar to the planet required for the broad debris disc, though noting (as in Section 3.3) that HR 8799 does not satisfy requirement (1) and so is not expected to have a maximized exocomet population.

The three requirements proposed above should be tested against numerical simulations, of which there are several in the literature. For example, Bonsor et al. (2012) did simulations of chains of planets between 5 and 50 au with masses of either Jupiter, Saturn, or Neptune. In all systems, most particles are scattered out, which is expected from requirement (1) because all systems have planets in the *ejected* region. They also found that while putting planets closer together increases the inward scattering rate, and that having high-mass planets does this faster, the overall fraction of the belt scattered in (referring to particles reaching <1 au) is both similar and a small fraction of $M_0/t_\star$ (see their fig. 9). This can be understood as lower mass planets may result in a larger fraction of the scattered material ending up at <1 au, but a higher mass planet may destabilize a larger fraction of the planetesimal belt. Regardless, these simulations are not optimized for inward scattering because they include a planet in the *ejected* region, and there is a finite source of planetesimals in the scattering region (requirement (3)). A closer example of simulations predicted to be optimized for inward scattering is given in Wetherill (1994); these simulations were not full *N*-body but, instead, used a Monte Carlo scattering approach based on the Öpik–Arnold method. That paper gave arguments similar to those above about the importance of reducing Jupiter's and Saturn's mass to stop the leak of particles being ejected, also pointing out that this allows the Earth to capture more comets into orbits interior to Jupiter. Their simulation B, which decreased Jupiter and Saturn to $15\,{\rm M}_\oplus$, found that this results in a factor of 100–1000 increase in the comet influx. Fig. 2 of Raymond & Bonsor (2014) also showed an increased scattering rate as the planet mass, in a system of five equal-mass planets, is decreased from 100 to $10\,{\rm M}_\oplus$, though the scattering rate decreased as the planet mass was decreased further to $5\,{\rm M}_\oplus$. Decreasing the planet mass further in the Wetherill (1994)

simulations did end up with a higher comet flux (their simulation D, which had 24 planets of 0.2–5 $M_\oplus$ in the 3.5–10 au region), but the character of the simulation had changed; these planets ended up on highly eccentric orbits, and the Earth also grew by a factor of 8, which is readily understood to arise because these planets are in the *accreted* regime, and were placed too close to prevent instability and scattering amongst the planets. Thus, for now, the extent to which comet influx can be increased by reducing planet masses below 10 $M_\oplus$ is unclear from simulations in the literature, and deserves further attention.

4.2.2 High long-period cometary flux

The requirements on planetary architecture to maximize the long-period comet flux are similar to those for Jupiter-family comets in Section 4.2.1. Requirement (1) for an absence of planets in the *ejected* region still stands, since once Galactic tides have perturbed Oort Cloud comets into the planetary system, they still need to pass the planets and can be ejected before reaching the innermost parts of the system. In numerical simulations which considered the effect of changing the mass of Jupiter, Horner, Jones & Chambers (2010) concluded that the rate of comets passed in from the Oort Cloud is reduced by the presence of a Jupiter-like ejector planet. Requirement (2) from Section 4.2.1 does not apply to comets torqued in from the Oort Cloud, for which tidal perturbations provide the inward torque. The replenishment requirement (3) from Section 4.2.1 still applies to this scenario but is perhaps most clearly rephrased as a requirement to maximize the mass implanted in the Oort Cloud (although the time taken for objects to reach the Oort Cloud and that to perturb them back to the inner system may argue for a specific configuration to explain replenishment at a particular stellar age). One way of achieving this is by placing the planets in a chain in which they all lie in the Oort Cloud region in Fig. 1, since all planets acting individually would act to scatter planetesimals in their vicinity towards the Oort Cloud. For example, placing all planets along the blue dotted line corresponding to a diffusion time-scale of 1 Gyr in Fig. 1 may be suitable. However, the constraints on the inner planets in the chain may in fact be less stringent, since as long as the planet masses increase sufficiently with orbital radius, the comets would be passed outwards along the chain, rather than inwards, with the consequence that it is the outermost planet in the chain that is important for understanding the eventual outcome. Just as late dynamical instabilities in the planetary system can enhance the exo-Kuiper belt comet flux, so also can stellar flybys in the short term enhance the long-period comet flux (Hills 1981; Fouchard et al. 2011), thus allowing high long-period comet influx rates in systems with planetary system architectures that result in low-mass Oort Clouds.

To test these proposed requirements, consider the simulations of Lewis et al. (2013) for the formation of the Oort Cloud in systems similar to the Solar system but reducing the masses of various planets down to either Saturn or Neptune mass. By the reasoning above, the resulting Oort Cloud from their simulations should not be too different to the current Oort Cloud because all simulations had Uranus and Neptune at their current masses, both of which Fig. 1 shows are able to scatter objects into the Oort Cloud, although a lower efficiency would be expected for simulations with more massive inner planets. Their fig. 1 shows that this is indeed the case, also confirming the ∼1 Gyr time-scale we predict for the creation of the Oort Cloud as well as its depletion by passing stars. Table 1 of Lewis et al. (2013) also gives the rates of long-period comets reaching <2 au, which were very similar for their simulations, although the rate was highest for the simulations in which all four giant planets had the Neptune mass. This configuration is closest to the optimal configuration we predict, but it may be possible to increase this rate further, since a Neptune-mass Jupiter and Saturn would still be in the *ejected* region. That is, these planets would have ejected material which could have ended up in the Oort Cloud had their masses been reduced to ∼5 $M_\oplus$ (or lower).

4.3 Debris in outer regions

Debris discs are most often detected by their far-IR emission which originates in dust at ≫10 au from the star. While this is most commonly interpreted as dust created in the collisional cascade of classical Kuiper belt analogues, this section explores how it might be possible to determine if the emission instead had a dominant scattering component, either a scattered disc (Section 4.3.1) or an Oort Cloud (Section 4.3.2).

4.3.1 Scattered disc

The possibility of observing debris that is being scattered by a planet, such as the component of the Kuiper belt that extends beyond Neptune and has orbits with pericentre close to Neptune, was already introduced in Section 3.3. This was used as a possible explanation for the broad debris disc of HR 8799, and the breadth of the disc is one observational manifestation of the scattering process. Simulations show that scattering processes cause an extended scattered disc to have a surface density distribution that falls off $\propto r^{-3.5}$ (Duncan et al. 1987). However, the observed profile of a scattered disc might be flatter than this due to collisional evolution, which preferentially erodes the inner parts of the distribution (Wyatt et al. 2010). Nevertheless, a scattered disc would be brightest at the inner edge, and detailed collisional modelling can be used to determine the expected radial profile.

Another potentially observable characteristic of such a disc is an absence of small dust grains. This is because most collisions occur at pericentre, which means that even large grains (i.e. even those with a radiation pressure coefficient $\beta < 0.01$) can be put on unbound orbits by radiation pressure, resulting in the size distribution being cut off at a size above that expected for a cascade of planetesimals on low-eccentricity ($e < 0.3$) orbits for which the cut-off is at $\beta \approx 0.5$ (Wyatt et al. 2010). This provides a means to test whether a debris disc originates in such a population, since a lack of small grains affects the temperature of the emission at a given radial location, and so may be, in evidence, as an unexpectedly low temperature either in the main ring or in the debris disc's halo (e.g. Matthews et al. 2014b). Such an interpretation is complicated, however, by the fact that a lack of small grains in the size distribution can also arise from a very low level of stirring (e.g. $e \ll 0.01$, Thébault & Wu 2008). While this affects only grains small enough to be put on elliptical orbits by radiation pressure (i.e. those with $0.1 < \beta < 0.5$), and the halo still comprises only small grains, constraints on the energy available in a collision to create a new surface area are another reason that small grains could be underabundant in systems with low levels of stirring (Krijt & Kama 2014; Thebault 2016).

If a star is concluded to have a scattered disc component (e.g. from the temperature and radial distribution of its debris disc emission), the properties of the scattering planet can be inferred from Fig. 1, given the stellar age, mass, and radius of the scattered disc's inner edge. A lack of small grains has been inferred for the outer 150-au ring of η Corvi (Duchêne et al. 2014), and also for other discs

imaged by *Herschel* (Pawellek et al. 2014; Pawellek & Krivov 2015). Application of this interpretation to η Corvi shows that at $\sim$1.4 Gyr this could still have a significant scattered disc population, of objects on their way to being implanted in the Oort Cloud, for a planet that is relatively low mass (i.e. with a scattering timescale of $\sim$10 Gyr, and so 1–10 $M_\oplus$). A more massive planet could also be the origin of the scattered disc, as long as it was put on to an orbit in the belt more recently. While it has been proposed that this system could be currently observed at an epoch analogous to that of the Solar system's Late Heavy Bombardment (Gomes et al. 2005), as an explanation that expands on that discussed in Section 4.1.3 for the unusually high quantities of hot dust in the system (Lisse et al. 2012), this may be ruled out by high-resolution imaging of the structure of the 150-au belt (Marino et al., 2016). Note, however, that the low temperature of the outer belt of η Corvi may also be explained by the composition of the debris, rather than by its dynamics (see discussion in Duchêne et al. 2014), and so it is premature to make claims of embedded planets in this system without more detailed analysis of the dust distribution.

A less extreme version of the scattered disc with its $r^{-3.5}$ profile can be made by decreasing the planet mass (or by looking at a younger star), since in this case the planetesimals may not yet have reached very high eccentricity orbits. Instead, the debris disc will appear broader than a typical disc, that is, the possibility discussed in Section 3.3. Examples of broad discs other than HR 8799 (Booth et al. 2016) include 61 Vir (Wyatt et al. 2012), γ Tri (Booth et al. 2013), and γ Dor (Broekhoven-Fiene et al. 2013). It may be hard to distinguish between a belt that was initially broad with low eccentricities and one which started narrower but was broadened by interactions with a planet. However, numerical simulations of this interaction might show that the surface density distribution has certain characteristics that can be compared with observations. As one example, fig. 1 of Booth et al. (2009) shows the surface density distribution in the Nice model of Gomes et al. (2005) at snapshots of before the instability (when the mass is concentrated in the belt), during the instability (when the belt is broad), and after the instability (when the belt is still broad but much depleted).

4.3.2 Mini-Oort Clouds

Consider the scenario described in Section 3.2 for the formation of Sedna-like objects applied to a larger population of detached objects. These objects would form a mini-Oort Cloud, that is, one with a radius of $\sim$1000 au. Since the orbital planes of this population would be randomized, they would form a spherical shell around the star, which if dense enough would collide to result in a collisional cascade and so dust (e.g. Howe & Rafikov 2014), which should emit at infrared-radio wavelengths and could be confused with a debris disc that would be interpreted as a Kuiper belt analogue. The detached disc population is not thought to be that significant in the Solar system, somewhere between 0.01 and 5 $M_\oplus$ depending on the size distribution (Brown, Trujillo & Rabinowitz 2004; Schwamb, Brown & Rabinowitz 2009; Trujillo & Sheppard 2014). However, extrasolar mini-Oort Clouds could be enhanced relative to ours, since the presence of Jupiter would have ejected many objects being scattered by Saturn before they would have reached our mini-Oort Cloud, and so systems without a Jupiter-like ejector would have enhanced versions of our detached disc population. The debris disc of Vega was originally interpreted as a spherical shell (Aumann et al. 1984), which might have been a reasonable explanation for the symmetrical dust distribution seen on the sky (Sibthorpe et al. 2010). However, this star is being viewed pole-on (Aufdenberg et al. 2006), and so the observed spherical symmetry of the dust distribution is more likely explained as a face-on viewing geometry of a planar debris disc that is aligned with the stellar equator. Thus, there is no convincing evidence that (mini-)Oort Clouds have been detected yet.

The existence of mini-Oort Clouds has already been proposed in the literature using a different formation mechanism, that is, planet–planet scattering (Raymond & Armitage 2013). This is not an outcome that was included in Fig. 2 because it likely results from a multiplanet interaction which causes the scattering planet to be moved far enough from the debris that further scattering interactions are prevented. The mechanism proposed here is different, since continued scattering by the planet is prevented by the tidal interaction of the debris with nearby stars (in the same way as our Oort Cloud formed), rather than by perturbations to the scattering planet. It is also relevant that Kaib, Roškar & Quinn (2011) found that the inner edge of the Oort Cloud can be strongly affected by radial migration of the host star through the Galaxy, and that encounters with field stars can be efficient at implanting objects on Sedna-like orbits if the host star spends significant time in dense environments.

4.4 Exoplanet populations

This section combines some thoughts on how scattering processes might be evident in the exoplanet populations. There is no point in repeating well-known conclusions (e.g. about the origin of the eccentric Jupiters), but there are prospects for discovering new scattered planets through direct imaging (Sections 4.4.1 and 4.4.2), or indeed for discovering those that have since been ejected (Section 4.4.3), and scattering processes may have direct relevance to the formation of super-Earth planets (Section 4.4.4).

4.4.1 Escaping planets

Section 3.3 already introduced the possibility that young stars may contain a population of planets that are in the process of being ejected from their systems in multiple scattering events off other close-in planets. However, Section 2.5 also pointed out one potential limitation on this population which is that scattered planets cannot be significantly more massive than the planet that scattered them. This implies that the known long-period giant planets, all of which are more massive than a few Jupiter mass (the detection threshold of current instrumentation), are unlikely to be this population of escaping planets (see also Bryan et al. 2016). Even if their systems do contain a several Jupiter mass planet orbiting closer in that is capable of scattering the planets to this distance, the escaping planet would have been put on to an unbound orbit on a timescale much shorter than the system age (multiplanet interactions notwithstanding).

The planetary system architecture which maximizes the population of escaping planets can be derived from Fig. 3; the scattering planets should all lie in the *escaping* shaded region (i.e. Neptune-mass planets at 5 au or Saturn-mass planets at 30–100 au), with no adjacent planets in the *ejected* region. As noted above, this restricts the scattered planets to be of similar or lower mass, which means they are too faint for detection with current instruments, unless surrounded by large quantities of dust (e.g. Kennedy & Wyatt 2011). If such escaping planets are discovered, then Fig. 3 provides a framework within which to consider what additional planets may be present in the system (e.g. see discussion in Section 3.3 about

the origin of Fomalhaut-b's orbit), albeit with caveats for possible multiplanet interactions.

A direct comparison of these predictions with the results of numerical simulations of planet–planet scattering (e.g. Chatterjee et al. 2008; Jurić & Tremaine 2008; Veras et al. 2009; Raymond et al. 2010) is hard because most simulations involved an initial population of planets with a range of masses drawn from a distribution. Consequently, a range of outcomes were found, not necessarily optimized to maximizing the scattered population. However, such simulations did demonstrate that such a population exists around young stars. For example, Veras et al. (2009) placed six planets at 3–7 au in the mass range of 3–3 $\times$ 10^4 $M_\oplus$ and found that most were ejected, but that some were still escaping at tens of Myr (see their fig. 1). This is expected from Fig. 3, since the assumed distribution means that one of the planets surely lies in the *ejected* region. While the few $>170\,M_\oplus$ planets in their escaping population (see their fig. 2) seem to contradict the prediction that the escaping planets cannot be massive, these likely originate from systems which also host massive inner planets, and the escaping planets may have been prevented from rapid ejection (which is the fate that Fig. 3 would otherwise predict) by encounters with other planets in the system. An escaping planet population is also seen in the simulations of Raymond et al. (2010), which, in agreement with the predictions of Fig. 1, showed that a larger fraction of three-planet systems with planets in (or close to) the escaping region (i.e. Neptune-mass planets) spend more time in a transitional ejection phase with pericentre larger than 5 au.

4.4.2 Exo-Sednas

As an addendum to the scenario discussed in Section 4.4.1, it is possible that the escaping planets never escaped but were pulled away from the inner planetary system by tidal forces which implanted them in the Oort Cloud at a distance appropriate for the cluster environment it was in. This could thus result in planets at an intermediate $\sim$1000 au distance (similar to the putative planet nine in the Solar system; Batygin & Brown 2016), which would be stable against further perturbations once the cluster has dissipated. Future surveys may find such planets on stable orbits and question whether they formed in situ, were captured from an orbit around a nearby star (Mustill, Raymond & Davies 2016), or were scattered out (as proposed here). One test of the latter hypothesis would be to search for the scattering planet, the properties of which can be predicted from Fig. 2 (i.e. they would be expected to lie in the Oort Cloud region on that figure) with the additional constraints of equation (11) (i.e. they would be more massive than the scattered planet), albeit with the caveat that multiple scattering planets may complicate the predictions.

The existence of such planets could also have implications for the inner planetary system. That is, if such planets are massive enough, and detached at a close enough separation from the star, these could have caused subsequent disruption to the inner planetary system. This is because, in the same way that the orbits of Oort Cloud comets are isotropic, tidal forces would have randomized the detached planet's orbital plane relative to that of its progenitor planetary system, and so the Oort Cloud planet could thus induce Kozai oscillations and so excite a large eccentricity in the inner planetary system. Indeed, Martin & Triaud (2016) invoked this mechanism as a way for a circumbinary planet to influence the orbit of its host stars. Such oscillations take time, however, and a multiplanet system may be stable against such perturbations, even if their time-scale is shorter than the age of the system.

4.4.3 Escaped planets

A further addendum to the scenario discussed in Section 4.4.1 is the possibility that planets might be detected after having been ejected from the system. Indeed, Jupiter-mass interstellar (or free floating) planets are possibly more common than main-sequence stars (Sumi et al. 2011), and it is possible that such planets formed in a circumstellar disc but were since ejected in scattering interactions with other planets in the system. This would imply that either planets capable of ejecting Jupiter-mass planets (i.e. those of comparable or greater mass, Section 2.5) are common, or the number of planets ejected per ejector is high, or that the interstellar planets have an origin in a different mechanism. The first of these possibilities can be assessed observationally, and current estimates would place the fraction of systems with Jupiter-mass planets at closer to 10 per cent than 100 per cent (Winn & Fabrycky 2015), though this cannot be claimed with any confidence, since the full range of parameter space has yet to be explored (in particular the occurrence rate of Jupiter-mass planets at large orbital radii is poorly constrained).

4.4.4 Super-Earth formation

Consider a system in which multiple embryos form within a few au. Fig. 1 shows that if these are nudged on to crossing orbits so that scattering ensues, then the result will be that the embryos collide and coalesce, until they are sufficiently separated. There have been many papers on this process so it is unnecessary to repeat here (see, e.g. Chambers 2001; Petrovich et al. 2014). However, one point to make is that the same applies to any solid mass that makes its way into the inner region. Thus, if we assume that planets in the outer region are scattering planetesimals, and potentially passing them inwards on to comet-like orbits, then if those planetesimals encroach into the growing super-Earth region, they will be accreted on to the super-Earth. The resulting exchange of angular momentum would make the super-Earth planet move out; how far depends on how much mass is accreted. Since the angular momentum of the planet scales as $\sim\mu m_{\rm p} a_{\rm p}^{1/2}$ (where $\mu = GM_\star$), and that gained from accreting a small mass dm at the pericentre of a high-eccentricity orbit is $\mu\,{\rm d}m\sqrt{2a_{\rm p}}$, the super-Earth planet would grow by this mechanism keeping $m_{\rm p}^{2(\sqrt{2}-1)}a_{\rm p}^{-1}$ constant, that is, along a track in Fig. 1 of $M_{\rm p} \propto a_{\rm p}^{1.2}$. Growth by this mechanism is fundamentally limited, however, by the rate at which mass can be scattered into the super-Earth's feeding zone, a topic discussed in Section 4.2. It is thus perhaps likely that scattering of planetesimals is an inefficient method of mass transfer.

It is also worth considering the implications of Fig. 1 for a model in which a super-Earth forms farther out and then migrates in (e.g. Alibert et al. 2006). In this case, the planet transitions from a region in which the material it encounters is destined for ejection to one where it starts to accrete everything it encounters. Indeed, the simulations of Payne et al. (2009) showed that a large fraction of planetesimals are not accreted on to the migrating planet in this process but, instead, end up in a broad scattered disc extending beyond where the planet started. Thus, we suggest from Fig. 1 that super-Earths might grow more efficiently in this way by evolving up a track on that figure that keeps them below the $v_{\rm esc} = v_{\rm k}$ line.

More generally, we can note that since the $v_{\rm esc} = v_{\rm k}$ line applies to the accretion of solid material, but not that of gas, the $v_{\rm esc}/v_{\rm k} = 1$

line should represent the maximum core mass for an object formed at that location. This explains why it is impossible to form Uranus and Neptune through collisional growth at their current locations (Levison & Stewart 2001). The discovery of solid planets at a large distance may thus provide a challenge for planet-formation models, which could be resolved if such planets form closer to the star and then migrate outwards, or if growth occurs through a mechanism such as pebble accretion (since gas drag can prevent the pebbles being ejected in the way discussed here; Levison, Kretke & Duncan 2015).

5 CONCLUSION

This paper considered the dynamical outcome for an object orbiting a star that is being scattered through close encounters with a planet. It was shown that, assuming a single low-eccentricity planet system, the outcome is divided into six main regions described in Section 2, and depends only on the mass and semimajor axis of the planet: accreted, ejected, remaining, escaping, Oort Cloud, and depleted Oort Cloud. While this division was known from the previous work of T93, this paper gives equal emphasis to all outcomes and considers the implications for the various components of extrasolar planetary systems that are much better known now. It also emphasizes the importance of the ratio of the planet's escape velocity to its Keplerian velocity in determining the outcome. After considering a few example systems and comparison with dynamical simulations in the literature (Section 3), this paper focuses on the types of planetary system architectures that favour specific outcomes (Section 4).

The outcome for scattering by terrestrial and super-Earth planets is accretion on to the planet, although mutual collisions with other objects undergoing scattering and eventual grinding into dust is another loss mechanism. Debris released in a giant impact involving the planet is a typical origin of a population undergoing such scattering. It was shown that the planet's mass and semimajor axis have a strong effect on the duration of detectability of giant impact debris which peaks at a specific planet mass and semimajor axis, the exact value of which depends on the detection threshold and wavelength of observation, as well as the spectral type of the star. Whereas the examples of giant impact debris proposed in the literature around A-type stars are found at radial locations compatible with expectations (i.e. at 4–6 au, implying progenitor planets of 3–10 $M_\oplus$), those found around Sun-like stars are found at $\ll$1 au much closer to the star than expected. This could indicate an absence of terrestrial planets beyond 1 au around Sun-like stars, emphasizing the potential of giant impact debris searches to constrain the frequency of habitable planets. However, for now we cannot rule out that giant impacts occur with equal frequency per logarithmic bin in planet mass and semimajor axis.

While the framework considered in this paper only applies to single-planet systems, scattering in a multiple-planet system can also be inferred by considering how each planet acts in isolation. This paper specifically considers which planetary system architectures favour the production of exocomets, identifying three principles that maximize exocomets being scattered in from an exo-Kuiper belt. Significant exocomet populations require a chain of closely spaced planets in which none of the planets is massive enough to favour ejection of objects that encounter it. Planet masses should not increase with distance from the star so that comets are passed in rather than out. Constant replenishment of the comet population is also required, which we suggest could be facilitated by a low-mass planet embedded in the exo-Kuiper belt. Similar principles apply to exocomets that arrive in the inner regions of the system from an exo-Oort Cloud. In this case, an absence of ejecting planets is also required, and the planet masses should be appropriate to maximize the amount of material that ends up in the exo-Oort Cloud.

Extrasolar debris discs are usually interpreted by analogy with the Solar system's classical Kuiper belt (i.e. objects on stable low-eccentricity orbits). Here we suggest the possibility that debris discs may have a significant scattered disc component (i.e. of objects with high eccentricities currently undergoing scattering with a planet). Such scattered discs could be inferred from the radial breadth of the debris disc and from a lack of small grains; e.g. the broad disc of HR 8799 could be caused by an embedded Saturn-mass planet. We also proposed that mini-Oort Clouds could result from a planetary system that was born in a dense cluster.

With many direct imaging campaigns currently searching for exoplanets at a large distance from their host star, this paper also considered the possibility of observing planets that are in the process of being ejected through interactions with an inner planetary system, or of seeing detached planets akin to Sedna in the Solar system. The framework presented in this paper readily provides predictions for the scattering planets that can be used in the interpretation of any such detections; for example, we showed how a 30-$M_\oplus$ planet at 32 au could explain the origin of the high eccentricity of the Fomalhaut-b orbit.

The value of the framework presented in this paper is in its simplicity, and as such its limitations should also be borne in mind. In particular, we did not consider the possibility that the planets are on eccentric orbits, which may aid scattering (e.g. Frewen & Hansen 2014), and lead to secular evolution of the planetary system, which could be important (e.g. Beust et al. 2014; Pearce & Wyatt 2014; Read & Wyatt 2016). Also, the planet mass versus semimajor axis diagram as presented claims to predict only the dominant outcome. Other outcomes are also possible but at a lower probability. Furthermore, only limited consideration was given to the dynamics of multiplanet systems. There is no substitute for *N*-body simulations which would provide a more definitive answer as to the outcome of scattering in a specific system. However, the framework presented herein provides a useful tool to interpret *N*-body simulations, which can also be used to devise planetary system architectures for specific outcomes, even if the predictions still need to be tested with more detailed simulations.

ACKNOWLEDGEMENTS

MCW, AB, and AS acknowledge the support of the European Union through European Research Council grant number 279973. APJ acknowledges support from NASA grant NNX16AI31G. AS is partially supported by funding from the Center for Exoplanets and Habitable Worlds. The Center for Exoplanets and Habitable Worlds is supported by the Pennsylvania State University, the Eberly College of Science, and the Pennsylvania Space Grant Consortium. This research has made use of the NASA Exoplanet Archive, which is operated by the California Institute of Technology, under contract with the National Aeronautics and Space Administration under the Exoplanet Exploration Program.

REFERENCES

Absil O. et al., 2006, A&A, 452, 237
Absil O. et al., 2013, A&A, 555, A104
Adams F. C., 2010, ARA&A, 48, 47
Alibert Y. et al., 2006, A&A, 455, L25
Akeson R. et al., 2013, PASP, 125, 989

Aufdenberg J. P. et al., 2006, ApJ, 645, 664
Aumann H. H. et al., 1984, ApJ, 278, L23
Bahcall J. N., Soneira R. M., 1980, ApJS, 44, 73
Batygin K., 2015, MNRAS, 451, 2589
Batygin K., Brown M. E., 2016, AJ, 151, 22
Beichman C. A. et al., 2005, ApJ, 626, 1061
Beust H., Morbidelli A., 2000, Icarus, 143, 170
Beust H. et al., 2014, A&A, 561, A43
Bonsor A., Wyatt M. C., 2012, MNRAS, 420, 2990
Bonsor A., Augereau J.-C., Thébault P., 2012, A&A, 548, A104
Bonsor A., Raymond S. N., Augereau J.-C., 2013, MNRAS, 433, 2938
Bonsor A., Raymond S. N., Augereau J.-C., Ormel C. W., 2014, MNRAS, 441, 2380
Booth M., Wyatt M. C., Morbidelli A., Moro-Martín A., Levison H. F., 2009, MNRAS, 399, 385
Booth M. et al., 2013, MNRAS, 428, 1263
Booth M. et al., 2016, MNRAS,
Bottke W. F., Jedicke R., Morbidelli A., Petit J.-M., Gladman B., 2000, Science, 288, 2190
Bottke W. F., Morbidelli A., Jedicke R., Petit J.-M., Levison H. F., Michel P., Metcalfe T. S., 2002, Icarus, 156, 399
Bowler B. P., 2016, PASP, 128, 102001
Boyajian T. S. et al., 2016, MNRAS, 457, 3988
Brasser R., Duncan M. J., 2008, Celest. Mech. Dyn. Astron., 100, 1
Brasser R., Schwamb M. E., 2015, MNRAS, 446, 3788
Brasser R., Duncan M. J., Levison H. F., 2006, Icarus, 184, 59
Brasser R., Duncan M. J., Levison H. F., 2007, Icarus, 191, 413
Brasser R., Duncan M. J., Levison H. F., 2008, Icarus, 196, 274
Broekhoven-Fiene H. et al., 2013, ApJ, 762, 52
Brown M. E., Trujillo C., Rabinowitz D., 2004, ApJ, 617, 645
Bryan M. L., Bowler B. P., Knutson H. A., Kraus A. L., Hinkley S., Mawet D., Nielsen E. L., Blunt S. C., 2016, ApJ, 827, 100
Canup R. M., Asphaug E., 2001, Nat, 412, 708
Chambers J. E., 2001, Icarus, 152, 205
Chatterjee S., Ford E. B., Matsumura S., Rasio F. A., 2008, ApJ, 686, 580
Chen C. H., Mittal T., Kuchner M., Forrest W. J., Lisse C. M., Manoj P., Sargent B. A., Watson D. M., 2014, ApJS, 211, 25
Contro B., Horner J., Wittenmyer R. A., Marshall J. P., Hinse T. C., 2016, MNRAS, 463, 191
Cotten T. H., Song I., 2016, ApJS, 225, 15
Defrère D. et al., 2015, ApJ, 799, 42
Defrère D. et al., 2016, ApJ, 824, 66
Dent W. R. F. et al., 2014, Science, 343, 1490
Dones L., Weissman P. R., Levison H. F., Duncan M. J., 2004, in Johnstone D., Adams F. C., Lin D. N. C., Neufeeld D. A., Ostriker E. C., eds, ASP Conf. Ser. Vol. 323, Star Formation in the Interstellar Medium: In Honor of David Hollenbach. Astron. Soc. Pac., San Francisco, p. 371
Dones L., Brasser R., Kaib N., Rickman H., 2015, Space Sci. Rev., 197, 191
Duchêne G. et al., 2014, ApJ, 784, 148
Duncan M. J., Levison H. F., 1997, Science, 276, 1670
Duncan M., Quinn T., Tremaine S., 1987, AJ, 94, 1330
Eiroa C. et al., 2013, A&A, 555, A11
Ertel S. et al., 2014, A&A, 570, A128
Evans N. W., Tabachnik S., 1999, Nature, 399, 41
Faber P., Quillen A. C., 2007, MNRAS, 382, 1823
Fabrycky D. C., Murray-Clay R. A., 2010, ApJ, 710, 1408
Ford E. B., Rasio F. A., 2008, ApJ, 686, 621
Fouchard M., Rickman H., Froeschlé C., Valsecchi G. B., 2011, A&A, 535, A86
Frewen S. F. N., Hansen B. M. S., 2014, MNRAS, 439, 2442
Fujiwara H., Onaka T., Yamashita T., Ishihara D., Kataza H., Fukagawa M., Takeda Y., Murakami H., 2012, ApJ, 749, L29
Genda H., Kobayashi H., Kokubo E., 2015, ApJ, 810, 136
Gillon M. et al., 2016, Nature, 533, 221
Goldreich P., Lithwick Y., Sari R., 2004, ApJ, 614, 497
Gomes R., Levison H. F., Tsiganis K., Morbidelli A., 2005, Nature, 435, 466
Goździewski K., Migaszewski C., 2014, MNRAS, 440, 3140
Heisler J., Tremaine S., 1986, Icarus, 65, 13
Heng K., Tremaine S., 2010, MNRAS, 401, 867
Higuchi A., Kokubo E., Mukai T., 2006, AJ, 131, 1119
Hills J. G., 1981, AJ, 86, 1730
Holmberg J., Flynn C., 2000, MNRAS, 313, 209
Horner J., Jones B. W., 2009, Int. J. Astrobiol., 8, 75
Horner J., Jones B. W., Chambers J., 2010, Int. J. Astrobiol., 9, 1
Howard A. W. et al., 2010, Science, 330, 653
Howe A. R., Rafikov R. R., 2014, ApJ, 781, 52
Ida S., Lin D. N. C., 2004, ApJ, 616, 567
Inamdar N. K., Schlichting H. E., 2016, ApJ, 817, L13
Jackson A. P., Wyatt M. C., 2012, MNRAS, 425, 657
Jackson A. P., Wyatt M. C., Bonsor A., Veras D., 2014, MNRAS, 440, 3757
Johnson B. C., Melosh H. J., 2012, Icarus, 217, 416
Jura M., 2005, ApJ, 620, 487
Jura M., 2011, AJ, 141, 155
Jurić M., Tremaine S., 2008, ApJ, 686, 603
Kaib N. A., Quinn T., 2008, Icarus, 197, 221
Kaib N. A., Roškar R., Quinn T., 2011, Icarus, 215, 491
Kalas P., Graham J. R., Clampin M., 2005, Nature, 435, 1067
Kalas P., Graham J. R., Fitzgerald M. P., Clampin M., 2013, ApJ, 775, 56
Kennedy G. M., Piette A., 2015, MNRAS, 449, 2304
Kennedy G. M., Wyatt M. C., 2011, MNRAS, 412, 2137
Kennedy G. M., Wyatt M. C., 2013, MNRAS, 433, 2334
Kennedy G. M., Wyatt M. C., 2014, MNRAS, 444, 3164
Kennedy G. M. et al., 2015, ApJS, 216, 23
Kenyon S. J., Bromley B. C., 2006, AJ, 131, 1837
Kiefer F., Lecavelier des Etangs A., Boissier J., Vidal-Madjar A., Beust H., Lagrange A.-M., Hébrard G., Ferlet R., 2014, Nature, 514, 462
Konopacky Q. M., Marois C., Macintosh B. A., Galicher R., Barman T. S., Metchev S. A., Zuckerman B., 2016, AJ, 152, 28
Krijt S., Kama M., 2014, A&A, 566, L2
Lagrange A.-M. et al., 2010, Science, 329, 57
Lawler S. M., Greenstreet S., Gladman B., 2015, ApJ, 802, L20
Lee M. H., Peale S. J., 2003, ApJ, 592, 1201
Levison H. F., Agnor C., 2003, AJ, 125, 2692
Levison H. F., Stewart G. R., 2001, Icarus, 153, 224
Levison H. F., Terrell D., Wiegert P. A., Dones L., Duncan M. J., 2006, Icarus, 182, 161
Levison H. F., Duncan M. J., Brasser R., Kaufmann D. E., 2010, Science, 329, 187
Levison H. F., Kretke K. A., Duncan M. J., 2015, Nature, 524, 322
Lewis A. R., Quinn T., Kaib N. A., 2013, AJ, 146, 16
Lisse C. M., Chen C. H., Wyatt M. C., Morlok A., 2008, ApJ, 673, 1106
Lisse C. M., Chen C. H., Wyatt M. C., Morlok A., Song I., Bryden G., Sheehan P., 2009, ApJ, 701, 2019
Lisse C. M. et al., 2012, ApJ, 747, 93
Löhne T. et al., 2012, A&A, 537, A110
Marino S. et al., 2016, MNRAS, in press
Marois C., Macintosh B., Barman T., Zuckerman B., Song I., Patience J., Lafrenière D., Doyon R., 2008, Science, 322, 1348
Marois C., Zuckerman B., Konopacky Q. M., Macintosh B., Barman T., 2010, Nature, 468, 1080
Martin D. V., Triaud A. H. M. J., 2016, MNRAS, 455, L46
Matthews B. C., Krivov A. V., Wyatt M. C., Bryden G., Eiroa C., 2014a, in > Beuther H., Klessen R. S., Dullemond C. P., Henning T., eds., Protostars and Planets VI, Observations, Modeling, and Theory of Debris Disks. Univ. Arizona Press, Tucson, AZ, p. 521
Matthews B., Kennedy G., Sibthorpe B., Booth M., Wyatt M., Broekhoven-Fiene H., Macintosh B., Marois C., 2014b, ApJ, 780, 97
Melis C., Zuckerman B., Rhee J. H., Song I., 2010, ApJ, 717, L57
Melis C., Zuckerman B., Rhee J. H., Song I., Murphy S. J., Bessell M. S., 2012, Nature, 487, 74
Meng H. Y. A. et al., 2014, Science, 345, 1032
Mennesson B. et al., 2014, ApJ, 797, 119
Morales F. Y. et al., 2009, ApJ, 699, 1067

Morales F. Y., Rieke G. H., Werner M. W., Bryden G., Stapelfeldt K. R., Su K. Y. L., 2011, ApJ, 730, L29
Morbidelli A., Wood B. J., 2015, Late Accretion and the Late Veneer. Wiley, New York
Mordasini C., Alibert Y., Benz W., 2009, A&A, 501, 1139
Moro-Martín A. et al., 2015, ApJ, 801, 143
Muñoz-Gutiérrez M. A., Pichardo B., Reyes-Ruiz M., Peimbert A., 2015, ApJ, 811, L21
Murray C. D., Dermott S. F., 1999, Solar System Dynamics. Cambridge Univ. Press, Cambridge
Murray N., Holman M., 1997, AJ, 114, 1246
Mustill A. J., Raymond S. N., Davies M. B., 2016, MNRAS, 460, L109
Nesvorný D., Jenniskens P., Levison H. F., Bottke W. F., Vokrouhlický D., Gounelle M., 2010, ApJ, 713, 816
Pawellek N., Krivov A. V., 2015, MNRAS, 454, 3207
Pawellek N., Krivov A. V., Marshall J. P., Montesinos B., Ábrahám P., Moór A., Bryden G., Eiroa C., 2014, ApJ, 792, 65
Payne M. J., Lodato G., 2007, MNRAS, 381, 1597
Payne M. J., Ford E. B., Wyatt M. C., Booth M., 2009, MNRAS, 393, 1219
Pearce T. D., Wyatt M. C., 2014, MNRAS, 443, 2541
Petrovich C., Tremaine S., Rafikov R., 2014, ApJ, 786, 101
Rasio F. A., Nicholson P. D., Shapiro S. L., Teukolsky S. A., 1992, Nature, 355, 325
Raymond S. N., Armitage P. J., 2013, MNRAS, 429, L99
Raymond S. N., Bonsor A., 2014, MNRAS, 442, L18
Raymond S. N., Armitage P. J., Gorelick N., 2010, ApJ, 711, 772
Read M. J., Wyatt M. C., 2016, MNRAS, 457, 465
Rhee J. H., Song I., Zuckerman B., 2007, ApJ, 671, 616
Rhee J. H., Song I., Zuckerman B., 2008, ApJ, 675, 777
Rogers L. A., 2015, ApJ, 801, 41
Schlichting H. E., Warren P. H., Yin Q.-Z., 2012, ApJ, 752, 8
Schwamb M. E., Brown M. E., Rabinowitz D. L., 2009, ApJ, 694, L45
Sibthorpe B. et al., 2010, A&A, 518, L130
Smith R., Churcher L. J., Wyatt M. C., Moerchen M. M., Telesco C. M., 2009a, A&A, 493, 299
Smith R., Wyatt M. C., Haniff C. A., 2009b, A&A, 503, 265
Smith R., Wyatt M. C., Haniff C. A., 2012, MNRAS, 422, 2560
Smullen R. A., Kratter K. M., Shannon A., 2016, MNRAS, 461, 1288
Steffl A. J., Cunningham N. J., Shinn A. B., Durda D. D., Stern S. A., 2013, Icarus, 223, 48
Stern S. A., Durda D. D., 2000, Icarus, 143, 360
Su K. Y. L. et al., 2009, ApJ, 705, 314
Sumi T. et al., 2010, ApJ, 710, 1641
Sumi T. et al., 2011, Nature, 473, 349
Tamayo D., 2014, MNRAS, 438, 3577
Thebault P., 2016, A&A, 587, A88
Thébault P., Wu Y., 2008, A&A, 481, 713
Thureau N. D. et al., 2014, MNRAS, 445, 2558
Traub W. A., 2012, ApJ, 745, 20
Tremaine S., 1993, in Phillips J. A., Thorsett S. E., Kulkarni S. R., eds, ASP Conf. Ser. Vol. 36, Planets Around Pulsars. Astron. Soc. Pac., San Francisco, p. 335 (T93)
Trujillo C. A., Sheppard S. S., 2014, Nature, 507, 471
Tsiganis K., Gomes R., Morbidelli A., Levison H. F., 2005, Nature, 435, 459
Udry S., Santos N. C., 2007, ARA&A, 45, 397
van Lieshout R., Dominik C., Kama M., Min M., 2014, A&A, 571, A51
Vanderburg A. et al., 2015, Nature, 526, 546
Veras D., Crepp J. R., Ford E. B., 2009, ApJ, 696, 1600
Veras D., Wyatt M. C., Mustill A. J., Bonsor A., Eldridge J. J., 2011, MNRAS, 417, 2104
Veras D., Mustill A. J., Gänsicke B. T., Redfield S., Georgakarakos N., Bowler A. B., Lloyd M. J. S., 2016, MNRAS, 458, 3942
Weinberg M. D., Shapiro S. L., Wasserman I., 1987, ApJ, 312, 367
Wetherill G. W., 1994, Ap&SS, 212, 23
Winn J. N., Fabrycky D. C., 2015, ARA&A, 53, 409
Wyatt M. C., 2003, ApJ, 598, 1321
Wyatt M. C., 2008, ARA&A, 46, 339
Wyatt M. C., Jackson A. P., 2016, Space Sci. Rev.,
Wyatt M. C., Dermott S. F., Telesco C. M., Fisher R. S., Grogan K., Holmes E. K., Piña R. K., 1999, ApJ, 527, 918
Wyatt M. C., Greaves J. S., Dent W. R. F., Coulson I. M., 2005, ApJ, 620, 492
Wyatt M. C., Smith R., Greaves J. S., Beichman C. A., Bryden G., Lisse C. M., 2007a, ApJ, 658, 569
Wyatt M. C., Smith R., Su K. Y. L., Rieke G. H., Greaves J. S., Beichman C. A., Bryden G., 2007b, ApJ, 663, 365
Wyatt M. C., Booth M., Payne M. J., Churcher L. J., 2010, MNRAS, 402, 657
Wyatt M. C., Clarke C. J., Booth M., 2011, Celest. Mech. Dyn. Astron., 111, 1
Wyatt M. C. et al., 2012, MNRAS, 424, 1206

APPENDIX A: STELLAR ENCOUNTERS

In Section 2.4, the time-scale for nearby stars to modify the orbit of a scattered object was calculated assuming that this was dominated by Galactic tides. Here we consider how including perturbations from stellar encounters would have changed (if at all) any of the resulting conclusions. For the case of the Solar system, Heisler & Tremaine (1986) concluded that the time-scales for stellar encounters to modify a comet's orbit scale in the same way as those for Galactic tides, but they are longer and so can be ignored. However, this conclusion may not apply to the broader range of system parameters considered in this paper, and moreover when calculating the perturbations from stellar encounters, it is important to note that the way these scale with system parameters depends on the rate of stellar encounters.

If the rate of stellar encounters is low enough that the resulting change in a comet's orbit is dominated by the single strongest stellar encounter, rather than by the cumulative effect of many weaker encounters (i.e. the perturbation is impulsive rather than diffusive), this leads to a mean-square change in the comet's specific angular momentum per orbit of (equation 37 of Heisler & Tremaine 1986)

$$\left\langle \Delta J^2 \right\rangle = 8 \times 10^{-30} \rho_{\rm s}^2 M_\star a^7 \quad \text{(A1)}$$

in au^4 yr^{-2}. In equation (A1), $\rho_{\rm s}$ is the local stellar mass density of nearby stars in units of 0.045 M$_\odot$ pc^{-3}, which is that appropriate for stars near the Sun (Bahcall & Soneira 1980; Holmberg & Flynn 2000), and assumes that the stellar mass distribution has the same shape as that near the Sun; see Table A1 for a summary of the units of parameters introduced in this appendix.

This assumption breaks down when the comet is far enough from the star that the smallest impact parameter expected over the comet's orbital period is inside the comet's orbit, that is, when the comet's semimajor axis $a > a_{\rm imp}$, where (see equation 35 of Heisler & Tremaine 1986)

$$a_{\rm imp} \approx 3.5 \times 10^4 M_\star^{1/7} \rho_{\rm s}^{-2/7} \sigma^{-2/7}, \quad \text{(A2)}$$

where σ is the velocity dispersion of nearby stars in units of 20 km s^{-1} (the value appropriate for stars near the Sun; Heisler

Table A1. Units of parameters introduced in Appendix A.

Parameter	Symbol	Units
Specific angular momentum	J	au^2 yr^{-1}
Local stellar mass density	$\rho_{\rm s}$	0.045 M$_\odot$ pc^{-3}
Velocity dispersion of nearby stars	σ	20 km s^{-1}
Impulsive/diffusive boundary	$a_{\rm imp}$	au

& Tremaine 1986). In this regime, the change per orbit is instead given by (equation 33 of Heisler & Tremaine 1986)

$$\left\langle \Delta J^2 \right\rangle = 3.5 \times 10^{-13} \rho_{\rm s} M_\star^{3/2} a^{7/2} \sigma^{-1}. \quad \text{(A3)}$$

Comparing equations (A1) and (A3) shows that for orbits at $a \gg a_{\rm imp}$ the diffusive perturbations from stellar encounters are much weaker than the impulsive approximation would have predicted. While this comparison also seems to imply that stellar encounters are stronger by a factor of $\sim$5 for orbits at the boundary between these regimes (i.e. at $a = a_{\rm imp}$) than would have been assumed by calculating their effect using the impulsive approximation, this factor is close to unity and independent of other parameters. Thus, we consider it more realistic that there is a smooth transition between the two regimes at a semimajor axis $\sim$1.6 times farther out than given by equation (A2), and that using the impulsive approximation will never underestimate the effect of stellar encounters, though it will overestimate it at $a \gg a_{\rm imp}$.

The mean-square change in the comet's specific angular momentum due to Galactic tides can also be calculated (equation 20 of Heisler & Tremaine 1986) as

$$\left\langle \Delta J^2 \right\rangle = 1.2 \times 10^{-29} \rho_0^2 M_\star^{-1} a^7. \quad \text{(A4)}$$

This means that the ratio of the perturbation (to a comet's angular momentum squared) from stellar encounters to that from Galactic tides is a factor of $0.65(\rho_{\rm s} M_\star/\rho_0)^2$ for $a < 1.6 a_{\rm imp}$, and lower than this for comets orbiting at larger semimajor axes. As such, we conclude that Galactic tides dominate over stellar encounters (which can thus be ignored) as long as

$$M_\star < 1.2 \rho_0/\rho_{\rm s}. \quad \text{(A5)}$$

Equation (A5) is satisfied for most of the systems considered in this paper, except that in Section 3.3.

The analysis presented in this paper (which assumed that Galactic tides dominate) can also be readily modified to account for stellar encounters. The simplest way to account for impulsive stellar encounters for systems which do not satisfy equation (A5) is to replace all instances of ρ_0 in the equations with $0.81 \rho_{\rm s} M_\star$. However, if such an analysis concludes that objects are placed by stellar encounters in an Oort Cloud at $a > 1.6 a_{\rm imp}$, then this calculation would have overestimated the effect of stellar encounters, which should instead have been considered in the diffusive regime. Replacing $a_{\rm f}$ in equation (5) with $1.6 a_{\rm imp}$ (from equation A2) shows that this applies to Oort Clouds formed by planets that are more massive than

$$M_{\rm p} = 2.9 M_\star^{17/28} a_{\rm p}^{3/4} \rho_0^{1/2} \rho_{\rm s}^{-3/14} \sigma^{-3/14}. \quad \text{(A6)}$$

Since planets more massive than equation (4) would still eject objects before placing them in the Oort Cloud, this means that only a narrow region of parameter space of planets beyond

$$a_{\rm p} = 800 M_\star^{-1} \rho_0^2 \rho_{\rm s}^{-2} \sigma^{-2} \quad \text{(A7)}$$

is potentially affected, though stellar encounters or Galactic tides may still implant objects in an Oort Cloud from scattering by planets in this region.

This paper has been typeset from a TEX/LATEX file prepared by the author.